IEEE Open Journal of Signal Processing

Received 31 December 2020; revised 25 April 2021; accepted 29 April 2021. Date of publication 6 May 2021; date of current version 15 June 2021. The review of this article was arranged by Associate Editor F. Cruz-Roldán.

Digital Object Identifier 10.1109/OJSP.2021.3078097

Effect of Generalized Improper Gaussian Noise and In-Phase/Quadrature-Phase Imbalance on Quadrature Spatial Modulation

MALEK M. ALSMADI [1], AYSE ELIF CANBILEN [2], NAJAH ABU ALI [3], AND SALAMA S. IKKI [1]

[1] Department of Electrical and Electronics Engineering, Lakehead University, Thunder Bay, Ontario P7B 5E1, Canada
[2] Department of Electrical and Electronics Engineering, Konya Technical University, Konya 42250, Turkey
[3] College of Information Technology, United Arab Emirates University, Al Ain, Abu Dhabi 15551, United Arab Emirates

CORRESPONDING AUTHOR: MALEK M. ALSMADI (e-mail: malsamdi@lakeheadu.ca).

ABSTRACT Quadrature spatial modulation (QSM) is a recently proposed multiple-input multiple-output (MIMO) wireless transmission paradigm that has garnered considerable research interest owing to its relatively high spectral efficiency. QSM essentially enhances the spatial multiplexing gain while maintaining all the inherent advantages of spatial modulation (SM). This work studies the effects of in-phase/quadrature-phase (I/Q) imbalance and improper Gaussian noise (IGN) on the performance of QSM. Considering a scenario where both receiver and transmitter operate under the effects of I/Q imbalance, we propose a novel receiver design that optimizes the system bit error rate (BER) when there is IGN at the receiver. Closed forms of the average pairwise error probability (APEP) and upper bound of the average BER formulas are derived. These formulas are derived considering the Beckmann fading channel model, where most well-known fading channel models can be considered special cases. The proposed designs demonstrate solid performance despite the effects of I/Q imbalance. In fact, these effects can be entirely eliminated if they exist at the receiver and significantly reduced at the transmitter. All analytical results were verified by computer simulations.

INDEX TERMS Improper Gaussian noise, I/Q imbalance, imperfect CSI, optimal detection, quadrature spatial modulation, Beckmann fading channel.

I. INTRODUCTION AND RELATED WORKS

The next-generation of wireless networks is expected to support a myriad of new demands, including higher data rate, lower latency, greater system capacity, massive connectivity, as well as increased power efficiency [1]. A key approach that can be taken towards the fulfillment of these expectations is the application of multiple-input multiple-output (MIMO) techniques [2]. Since they can ensure a remarkable capacity gain and provide high data rates, MIMO techniques have played a major role in recent standards such as long-term evolution (LTE), LTE-advanced, and worldwide interoperability for microwave access (WiMAX) [3]. The significant challenges facing next-generation MIMO technology can be enumerated as follows: 1) designing multi-antenna transmission schemes with reduced complexity and number of radio frequency (RF) chains, 2) avoiding inter-antenna synchronization and inter-channel interference (ICI), 3) improving energy efficiency (EE) [2].

Considering the above, spatial modulation (SM) was introduced as a flexible solution for the main issues with traditional MIMO communications [4]. SM extends the conventional two-dimensional complex signal plane to a third dimension (i.e., the spatial dimension). This unique approach uses the transmitter antenna (TA) index as an supplementary information source. Since only one TA is activated at each transmission time instant, *i.e.,* only one RF chain is operated. SM not only provides high EE but also eliminates the ICI as well as the requirement for TA synchronization. Moreover, a high spectral efficiency (SE) is achieved since the transmitted symbol carries a greater number of information bits using

the same time duration [4]. Single-RF SM offers high energy efficiency with one active antenna. Unfortunately, the spectral efficiency has a slow logarithmic growth when increasing the number of transmit antennas. Hence, generalized SM (GSM) exploits more than one active antenna to transmit more than one symbol simultaneously. The work in [5] proposed a less complex SM detection algorithm. Particularly, this work utilized the compressive sensing principle to present a detector for the multiple-access SM channels with a large-scale antenna at the base station, which allows a reduction in the signal processing load. More information about SM can be found in the survey papers [6], [7].

Quadrature SM (QSM) was proposed in [8] to further enhance the SE of SM. The receiver complexities of SM and QSM schemes are equal and depend on the considered SE. On the other hand, in QSM, the spatial constellation symbols of conventional SM are expanded to include two spatial dimensions, each separately transmitting the real and imaginary parts of a conventional amplitude/phase modulation (APM) data symbol. Since this transmission procedure is realized in an orthogonal manner, ICI is avoided in QSM as well. Additionally, the number of bits conveyed by active TA indices is twice that of SM [8]. There are many extensions for QSM in the literature. For instance, Generalized QSM (GQSM) was proposed to further increase the SE of the QSM by activating more than one transmit antenna in I or Q domain [9]. Also, generalized precoding-aided quadrature spatial modulation (GPQSM), was proposed as a novel technique that only requires the channel state information (CSI) at the transmitter side [10]. The work in [11] proposed a less complex QSM detection algorithm. Particularly, the proposed detector utilizes the set of most probable active transmit antennas and the corresponding possible transmission patterns. After that, Maximum likelihood (ML) based detection is used to determine the transmitted complex data vector. Also, the adoption of QSM for large-scale MIMO configurations was presented in [12], where a low-complexity decoder was proposed and analyzed.

Hardware impairments (HWIs), such as imperfect manufacturing of the high-power amplifier, I/Q imbalance at the RF front-end, and the non-linearity of the low noise amplifier can dramatically degrade the system performance [13]. I/Q imbalance is one of the most serious sources of analog impairments in high-speed communication networks, and is due to an insufficient rejection of the image frequency band [14], [15], [16]. Furthermore, HWIs have a negative impact on system secrecy [17]. It has also been reported that I/Q imbalance effects are more severe at higher carrier frequencies such as millimeter-wave bands [18], which are expected to play a major role in 5 G and beyond communication systems [19].

Examining the effects of HWIs on system performance and choosing proper detection designs both require a general model that can represent the wide range of HWIs. These HWIs are modeled mostly in the literature as proper Gaussian terms at the transmitter and receiver [13], [20]–[22]. In several recent works, however, more general models were used to describe the HWIs, namely improper Gaussian random variables (RVs) [23]. In addition, a more generalized model of additive white Gaussian noise (AWGN) at the receiver was conceived, where the noise was assumed to be improper Gaussian noise (IGN) [24], [25].

Maximum likelihood (ML) detector behavior in the presence of IGN was considered for the first time in [24] and [25]. The work in [24] confirmed that using the ML detector to exploit the improperness of the Gaussian noise leads to a decrease in the error probability when detecting the binary signals. In [25], a general likelihood test was performed to detect the target patterns in multi-band spectral images. The results indicated that more computational time is required to detect the patterns in a system operating under the effects of IGN. In [26], the optimal ML receiver of the single-input multiple-output (SIMO) system is used to detect the quadrature amplitude modulation symbols affected by IGN. It was shown that the ML receiver under the assumption of IGN outperforms the one under the assumption of proper Gaussian noise (PGN).

The issue of co-channel interference (CCI) and its negative impact on the performance of a QSM system was studied in [27]. The obtained results proved that QSM is superior to SM in the presence of CCI for the same system setup. The effect of imperfect CSI on the overall system performance of the QSM receiver was discussed in [28], and it was emphasized that not only was the QSM system considerably more resilient to channel estimation errors than the conventional SM system, it was also able to achieve higher SE. In addition to this, the results demonstrated that, in the presence of imperfect CSI, QSM requires 3-5 decibel (dB) less in signal power than the conventional SM for the same SE and error performance without any additional receiver complexity.

Since future wireless standards are expected to be based on millimeter-wave (mmWave) and large scale MIMO technologies, the combination of mmWave and QSM schemes was studied in [29], where significant performance enhancements were achieved under different system and channel configurations. In [30], the capacity analysis for the QSM scheme over a three-dimensional mmWave MIMO wireless communication system was provided.

The work in [31] proposed a low-complexity compensation scheme to tackle the problem of I/Q imbalance at the base station in a massive MIMO system. This method was also used to mitigate I/Q imbalance encountered in wideband mmWave transmitters. The authors in [32], [33] showed that I/Q imbalance has a negative impact on the SM error performance. Moreover, they proposed a receiver design that can mitigate the effects of I/Q at an SM receiver. However, they assumed the presence of PGN at the receiver, meaning that their design cannot be applied in the case of IGN. In addition, this design cannot be applied to the more general case of SM, i.e., the QSM system. Surprisingly, the effects of I/Q imbalance on QSM transmission have been discussed only once in the literature. In [34], the performance of a QSM

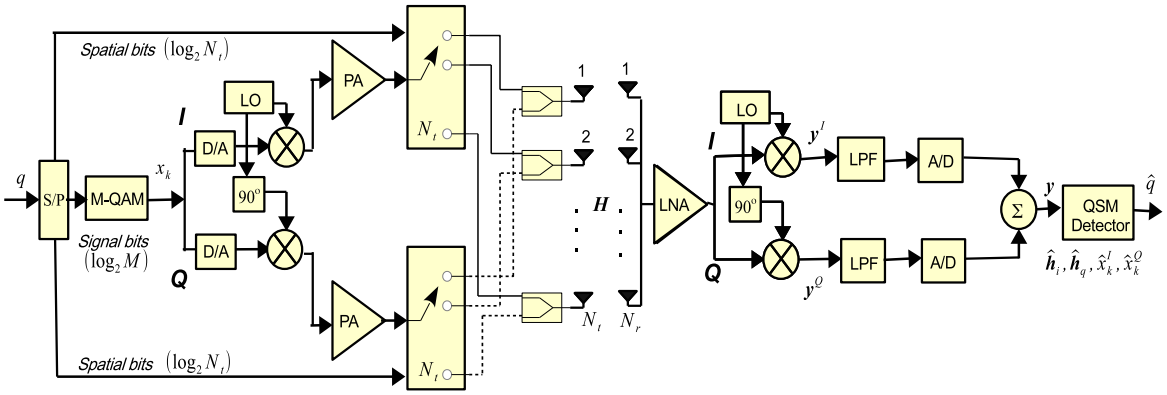

FIGURE 1. QSM wireless communication system employing a direct conversation at the transmitter and receiver.

receiver under the effects of I/Q imbalance was examined, analyzing the performance of the pairwise error probability (PEP) and the average bit error rate (ABER). However, this study was realized by utilizing a non-optimal solution under the assumption of perfect CSI.

To the best of our knowledge, no work in the literature proposed an ideal receiver design that can mitigate the effects of I/Q imbalance on QSM systems and accurately treat the IGN at the receiver. Therefore, in this paper, the traditional ML detector design is accurately adapted for QSM systems that suffer from I/Q imbalance at the transmitter and receiver sides as well as imperfect CSI at the receiver. In addition, the AWGN at the receiver is assumed to be IGN. An optimum ML detection method is proposed to address the effects of self-interference and signal distortion caused by I/Q imbalance. This method is also used to appropriately treat the impact of IGN at the receiver. Average PEP and ABER are defined, and an asymptotic approximation is presented. The simulation results match the analytical derivations, corroborating the presented analysis. The results demonstrate that the proposed ML detector design is in fact superior to the traditional ML detector. *Notation:* $(\cdot)^{-1}$ and $|\ |$ indicate matrix inverse and determinant respectively. $[\ .\ ]^T$ is the vector transpose. $(.)^I$ and $(.)^Q$ denote the I and Q components. The magnitude of the complex number is represented by $|\cdot|^2$. $\mathcal{CN}(\mu, \sigma^2)$ represents the complex Gaussian random variable distribution with mean μ and variance σ^2. $\mathcal{CN}(\boldsymbol{\mu}, \boldsymbol{\Gamma})$ represents the complex random Gaussian vector with mean $\boldsymbol{\mu}$ and covariance matrix $\boldsymbol{\Gamma}$. ρ_i is the correlation between the real and imaginary parts of a complex random variable i. P(.) is the probability of the event. $Q(x) = \frac{1}{\sqrt{2\pi}} \int_x^\infty \exp\left(\frac{-u^2}{2}\right) du$.

The rest of this paper is organized as follows: Section II describes the QSM system and channel models. Section III follows with a discussion on the accumulative noise at the receiver. Next, Section IV outlines the receiver design. Section V discusses the performance analysis for the presented model. Section VI provides the numerical analysis and Section VII concludes this paper.

II. SYSTEM AND CHANNEL MODELS

Consider a QSM wireless communication system employing a direct down-conversion (DDC), also referred to as homodyne architecture transceiver in the RF front-end as given in Fig. 1. First of all, the incoming data stream q is partitioned into groups, each of which has $m = \log_2(N_t^2 M)$ bits at the transmitter side (M is the modulation order of complex constellations and N_t is the number of TAs). These groups are further divided into three blocks of bits, two of which are used for spatial mapping and the remaining one for ordinary signal mapping. Each signal bit block has $\log_2(M)$ bits and modulates a conventional amplitude/phase modulation symbol, e.g., M-QAM.

During the homodyne up-conversion stage, the baseband digital signal x_k, $k = [1, \ldots, M]$, is first converted to an analog one. Then, x_k^I modulates the in-phase (I) part (cosine) of the carrier while x_k^Q modulates the quadrature-phase (Q) part (sine). After amplifying the I and Q parts of the signal with power amplifiers (PAs), they are mapped into transmitter indices by using spatial bits. These act as controllers to enable or disable the TAs at each specific time instant using a QSM demultiplexer. The RF signal goes through an $N_r \times N_t$ sized fading channel characterized by $\mathbf{H}$, where N_r is the number of receiver antennas. The columns of the channel matrix, $\boldsymbol{h}_i$, represent the complex fading coefficients between the i^{th} transmitter and all receiver antennas while $h_{l,i}$ represents the complex fading coefficients between the i^{th} transmitter and l^{th} receiver antennas.

In this work, we use Beckmann fading channels but make no assumptions regarding the statistics of the channel amplitudes and phases. It is worth keeping in mind that most well-known fading channel models can be considered special cases. Allowing the real and imaginary parts of the channel matrix elements to have different means and variances, or to be correlated, leads to a more general fading channel model. More detail concerning Beckmann fading channels can be found in Appendix B. Based on this, the elements of the channel matrix $\mathbf{H}$ can be modeled as $\mathcal{CN}(\boldsymbol{\mu}_{h_{l,i}}, \boldsymbol{\sigma}^2_{h_{l,i}})$ where the mean vector and the covariance matrix of each element

are given by $\boldsymbol{\mu}_{\boldsymbol{h_{l,i}}}$ and $\boldsymbol{\sigma}^{\boldsymbol{2}}_{\boldsymbol{h_{l,i}}}$, respectively

$$\boldsymbol{\mu}_{\boldsymbol{h_{l,i}}} = \begin{bmatrix} \mu_{h^I_{l,i}} & \mu_{h^Q_{l,i}} \end{bmatrix},$$
$$\boldsymbol{\sigma}^{\boldsymbol{2}}_{\boldsymbol{h_{l,i}}} = \begin{bmatrix} \sigma^2_{h^I_{l,i}} & \rho_{h_{l,i}}\sigma^Q_{h_{l,i}}\sigma^I_{h_{l,i}} \\ \rho_{h_{l,i}}\sigma^Q_{h_{l,i}}\sigma^I_{h_{l,i}} & \sigma^2_{h^Q_{l,i}} \end{bmatrix}. \quad (1)$$

At the receiver side, the received signal is first amplified by a low-noise amplifier (LNA) and then, quadrature mixing is applied by local oscillators (LO). Afterwards, the signal on each branch passes through a low pass filter (LPF) and an analog to digital converter (ADC) converter. Following these operations, the QSM detector recovers the whole information block (activated antenna indices and the transmitted symbol). The noise vector $\boldsymbol{n} = [n_1, \ldots, n_{N_r}]^T$ at the receiver antennas has uncorrelated and identical components at each receiver. Here, being identical means that they have the same mean vector and covariance matrix. The noise at each receiver is improper and follows $\mathcal{CN}(\mathbf{0}, \boldsymbol{\sigma}^{\boldsymbol{2}}_{\boldsymbol{n_l}})$, where the covariance matrix $\boldsymbol{\sigma}^{\boldsymbol{2}}_{\boldsymbol{n_l}}$ is given by

$$\boldsymbol{\sigma}^{\boldsymbol{2}}_{\boldsymbol{n_l}} = \begin{bmatrix} \sigma^2_{n_l{}^I} & \rho_{n_l}\sigma^I_{n_l}\sigma^Q_{n_l} \\ \rho_{n_l}\sigma^I_{n_l}\sigma^Q_{n_l} & \sigma^2_{n_l{}^Q} \end{bmatrix}. \quad (2)$$

A. IMPERFECT CSI MODEL

In realistic wireless communication conditions, exact CSI is not available at the receiver, so channel estimators (e.g., least square or minimum mean square error estimators) can be used to offer a reasonable approximation. In this case, the $\hat{\mathbf{H}}$ estimate can be modeled as

$$\mathbf{H} = \hat{\mathbf{H}} + \mathbf{H}_e\ , \quad (3)$$

where $\mathbf{H}_e$ is the channel estimation error matrix. It must be noted, however, that, as shown in [35], the fading channel component $h_{l,i}$ and its estimated versions $\hat{h}_{l,i}$ are jointly ergodic and stationary. Therefore, the related channel estimation error $e_{l,i}$ can be modeled as $\mathcal{CN}(\mathbf{0}, \boldsymbol{\sigma}^{\boldsymbol{2}}_{\boldsymbol{e_{l,i}}})$, where the covariance matrix $\boldsymbol{\sigma}^{\boldsymbol{2}}_{\boldsymbol{e_{l,i}}}$ is given by

$$\boldsymbol{\sigma}^{\boldsymbol{2}}_{\boldsymbol{e_{l,i}}} = \begin{bmatrix} \sigma^2_{e^I_{l,i}} & \rho_{e_{l,i}}\sigma^Q_{e_{l,i}}\sigma^I_{e_{l,i}} \\ \rho_{e_{l,i}}\sigma^Q_{e_{l,i}}\sigma^I_{e_{l,i}} & \sigma^2_{e^Q_{l,i}} \end{bmatrix}. \quad (4)$$

From (4) and (1), the estimated channel $\hat{\mathbf{H}}$ is a Beckmann channel as in (1) with

$$\boldsymbol{\mu}_{\boldsymbol{\hat{h}_{l,i}}} = \begin{bmatrix} \mu_{h^I_{l,i}} & \mu_{h^Q_{l,i}} \end{bmatrix},$$
$$\sigma^2_{\hat{h}^I_{l,i}} = \sigma^2_{h^I_{l,i}} + \sigma^2_{e^I_{l,i}},$$
$$\sigma^2_{\hat{h}^Q_{l,i}} = \sigma^2_{h^Q_{l,i}} + \sigma^2_{e^Q_{l,i}},$$
$$\rho_{\hat{h}_{l,i}} = \frac{\rho_{h_{l,i}}\sigma^Q_{h_{l,i}}\sigma^I_{h_{l,i}} + \rho_{e_{l,i}}\sigma^Q_{e_{l,i}}\sigma^I_{e_{l,i}}}{\sqrt{\sigma^2_{\hat{h}^I_{l,i}}\,\sigma^2_{\hat{h}^Q_{l,i}}}}. \quad (5)$$

B. TRANSMITTER AND RECEIVER I/Q IMBALANCE MODEL

The direct-conversion architecture is widely used for low-cost, low-power transceivers in modern wireless systems. However, due to LO, there a few things we must consider: 1) The I and Q angles at the transmitter or receiver signals might not be exactly perpendicular. This is the phase imbalance. 2) Small variations might exist between the I and Q amplitudes at the transmitter or receiver. This is the amplitude imbalance. The consequence is that I/Q imbalance can significantly affect the system's performance by changing the signal at the transmitter or corrupting it at the receiver.

Three main reasons render the effects of I/Q imbalance critical for next-generation communication systems. First, these effects worsen with larger signal constellations since the probability of incorrect detection increases as the distances between the constellations decrease. This is not very compatible with next-generation requirements, where denser constellations are required to obtain higher data rates. For example, IEEE 802.11ax swells constellation density by adding 1024-QAM to support more efficient communications [36]. Second, next generation communication networks require a massive number of connected devices. This can be supported by manufacturing low-cost transceivers, however at the cost of poor quality [37]. Third, new technologies such as mmWave might not always able to meet the standard requirements for acceptable levels of I/Q imbalance [38].

Now, considering the frequency-independent I/Q imbalance model [32], [39], the transmitted signal can be given as

$$\tilde{x}_k = G_1 x_k + G_2 {x_k}^*, \quad (6)$$

where $G_1 = \frac{1}{2}(1 + \xi_t e^{j\beta_t})$ and $G_2 = \frac{1}{2}(1 - \xi_t e^{j\beta_t})$ are I/Q imbalance parameters at the transmitter. Here, ξ_t and β_t represent the amplitude and the phase mismatches in the up-conversion process, respectively. It can be noted that for perfect I/Q balance, the amplitude imbalance parameter $\xi_t = 1$ and the phase imbalance parameter $\beta_t = 0$. Consequently, $G_1 = 1$, $G_2 = 0$ and the transmitted signal is x_k. Now, designating $G_c = (G^Q_1 - G^Q_2)$ and $G_d = (G^I_1 - G^I_2)$, and noting that $G^I_1 + G^I_2 = 1$ and $G^Q_1 + G^Q_2 = 0$, $\tilde{x}^I_k$ and $\tilde{x}^Q_k$ can be given as

$$\tilde{x}^I_k = x^I_k - x^Q_k G_c, \quad \tilde{x}^Q_k = x^Q_k G_d. \quad (7)$$

Considering the effects of the I/Q imbalance model at the receiver side, the received baseband signal at l^{th} receiver antenna is

$$y_l = K_1\left[\sqrt{E}(h_{l,i}\tilde{x}^I_k + jh_{l,q}\tilde{x}^Q_k) + n_l\right] + K_2\left[\sqrt{E}(h_{l,i}\tilde{x}^I_k + jh_{l,q}\tilde{x}^Q_k) + n_l\right]^*, \quad (8)$$

where $\{i, q\} \in \{1, \ldots, N_t\}$ and represent the indices of the activated QSM TAs, $l = \{1, \ldots, N_r\}$. Here $h_{l,i}$ and $h_{l,q}$ are the corresponding complex channel coefficients, E is the transmitted signal energy, $K_1 = \frac{1}{2}(1 + \xi_r e^{-j\beta_r})$ and $K_2 = \frac{1}{2}(1 - \xi_r e^{j\beta_r})$ are I/Q imbalance coefficients at the receiver. ξ_r and β_r represent the amplitude and phase mismatches in the down-conversion process, respectively. Now, denoting $K_c = K^Q_1 +$

K_2^Q and $K_d = K_1^I - K_2^I$, and noting that $K_1^I + K_2^I = 1$ and $K_1^Q - K_2^Q = 0$, (8) can be rewritten after some mathematical operations involving (3) as

$$\begin{aligned} y_l &= \sqrt{E}\{\tilde{h}_{l,i}^I(x_k^I - x_k^Q G_c) - \tilde{h}_{l,q}^Q x_k^Q G_d\} + n_l^I \\ &+\sqrt{E}\{e_{l,i}^I(x_k^I - x_k^Q G_c) - e_{l,q}^Q x_k^Q G_d\} + j\{n_l^I K_c + n_l^Q K_d\} \\ &+j\sqrt{E}\{\tilde{h}_{l,i}^I(x_k^I - x_k^Q G_c)K_c + \tilde{h}_{l,i}^Q(x_k^I - x_k^Q G_c)K_d\} \\ &+j\sqrt{E}\{e_{l,i}^I(x_k^I - x_k^Q G_c)K_c + e_{l,i}^Q(x_k^I - x_k^Q G_c)K_d\} \\ &+j\sqrt{E}\{\tilde{h}_{l,q}^I x_k^Q G_d K_d + e_{l,q}^I x_k^Q G_d K_d - e_{l,q}^Q x_k^Q G_d K_c\} \\ &+j\sqrt{E}\{-\tilde{h}_{l,q}^Q x_k^Q G_d K_c\}. \end{aligned} \tag{9}$$

III. ACCUMULATIVE NOISE AT THE RECEIVER

The accumulative noise is affected by the I/Q parameters at the transmitter and receiver, the channel estimation error, and the noise at the receiver. If the noise at the receiver is improper (which is the more general case), then the channel estimation error is assumed to be improper as well. From (9), the noise component of y_l, which is a zero-mean complex Gaussian random variable (RV), is given by

$$\begin{aligned} \tilde{n}_l &= n_l^I + j\{n_l^I K_c + n_l^Q K_d\} + \sqrt{E}\{e_{l,i}^I(x_k^I - x_k^Q G_c)\} + \\ &j\sqrt{E}\{e_{l,i}^I(x_k^I - x_k^Q G_c)K_c + e_{l,q}^I x_k^Q G_d K_d - e_{l,q}^Q x_k^Q G_d K_c\} \\ &- \sqrt{E}\{e_{l,q}^Q x_k^Q G_d\} + j\sqrt{E}\{e_{l,i}^Q(x_k^I - x_k^Q G_c)K_d\}. \end{aligned} \tag{10}$$

The improper characteristics of a complex RV depends on the existence at least one of the following conditions [40]: i) the I and Q parts are correlated and/or ii) the I and Q parts are not identical (i.e., do not have the same variances). In order to analyze the improper characteristics of $\tilde{n}_l$, these two conditions need to be checked. It can be concluded that the accumulative noise is improper because we assumed in our model that the noise $\tilde{n}_l$ is improper. Based on this, the variances of the real and imaginary parts of n_l are calculated as follows

$$\begin{aligned} \sigma_{\tilde{n}_l^I}^2 &= \sigma_{n_l{}^I}^2 + E(x_k^I - x_k^Q G_c)^2\sigma_{e_{l,i}^I}^2 + E(x_k^Q G_d)^2\sigma_{e_{l,q}^Q}^2, \\ \sigma_{\tilde{n}_l^Q}^2 &= \sigma_{n_l{}^I}^2 K_c^2 + \sigma_{n_l{}^Q}^2 K_d^2 + 2\rho_{n_l} K_c K_d \sigma_{n_l^I}^I \sigma_{n_l^Q}^Q \\ &+E(x_k^I - x_k^Q G_c)^2\sigma_{e_{l,i}^I}^2 K_c^2 + E(x_k^I - x_k^Q G_c)^2\sigma_{e_{l,i}^Q}^2 K_d^2 \\ &+2E\rho_{l,i}^e K_c K_d (x_k^I - x_k^Q G_c)^2 \sigma_{e_{l,i}^Q}^Q \sigma_{e_{l,i}}^I \\ &+E(x_k^Q G_d)^2\sigma_{e_{l,q}^Q}^2 K_c^2 + E(x_k^Q G_d)^2\sigma_{e_{l,q}^I}^2 K_d^2 \\ &+2E\rho_{l,q}^e K_c K_d (x_k^Q G_d)^2 \sigma_{e_{l,q}^Q}^Q \sigma_{e_{l,q}}^I. \end{aligned} \tag{11}$$

The correlation coefficient can be calculated using (11) as ($\mathbb{E}\{\tilde{n}_l{}^I\} = \mathbb{E}\{\tilde{n}_l{}^Q\} = 0$)

$$\varrho_l = \frac{\mathbb{E}\{\tilde{n}_l{}^I \tilde{n}_l{}^Q\}}{\sqrt{\sigma_{\tilde{n}_l{}^I}^2 \sigma_{\tilde{n}_l{}^Q}^2}}, \tag{12}$$

where $\mathbb{E}\{\tilde{n}_l{}^I \tilde{n}_l{}^Q\}$ is given by

$$\begin{aligned} \mathbb{E}\{\tilde{n}_l{}^I \tilde{n}_l{}^Q\} &= \rho_{n_l}\sigma_{n_l^I}^I \sigma_{n_l^Q}^Q K_d + E(x_k^I - x_k^Q G_c)^2\sigma_{e_{l,i}{}^I}^2 K_c \\ &+E(x_k^Q G_d)^2\sigma_{e_{l,q}{}^Q}^2 K_c - E(x_k^Q G_d)^2\rho_{l,i}^e \sigma_{e_{l,i}^Q}^Q \sigma_{e_{l,i}^I}^I K_d \\ &+E(x_k^I - x_k^Q G_c)^2\rho_{l,i}^e \sigma_{e_{l,i}^Q}^Q \sigma_{e_{l,i}^I}^I K_d + \sigma_{n_l{}^I}^2 K_c\,. \end{aligned} \tag{13}$$

Now, noting that the channel estimation errors $e_{l,i}$ and $e_{l,q}$ are uncorrelated and identical, (11) and (13) can be rewritten as (14) and (15) respectively

$$\begin{aligned} \sigma_{\tilde{n}_l^I}^2 &= \sigma_{n_l{}^I}^2 + E(x_k^I - x_k^Q G_c)^2\sigma_{e^I}^2 + E(x_k^Q G_d)^2\sigma_{e^Q}^2, \\ \sigma_{\tilde{n}_l^Q}^2 &= E\sigma_{e^I}^2\left[(x_k^I - x_k^Q G_c)^2 K_c^2 + (x_k^Q G_d)^2 K_d^2\right] + \sigma_{n_l{}^I}^2 K_c^2 \\ &+ E\sigma_{e^Q}^2\left[(x_k^I - x_k^Q G_c)^2 K_d^2 + (x_k^Q G_d)^2 K_c^2\right] \\ &+ \sigma_{n_l{}^Q}^2 K_d^2 \\ &+ 2E\rho_e K_c K_d\left[(x_k^I - x_k^Q G_c)^2 + (x_k^Q G_d)^2\right]\sigma_e^I \sigma_e^Q, \end{aligned} \tag{14}$$

$$\begin{aligned} \mathbb{E}\{\tilde{n}_l{}^I \tilde{n}_l{}^Q\} &= \sigma_{n_l{}^I}^2 K_c + \rho_{n_l}\sigma_{n_l^I}^I \sigma_{n_l^Q}^Q K_d \\ &+ EK_c\left[\sigma_{e_I}^2(x_k^I - x_k^Q G_c)^2 + \sigma_{e_Q}^2(x_k^Q G_d)^2\right] \\ &+ E\rho_e\sigma_e^Q\sigma_e^I K_d\left[(x_k^I - x_k^Q G_c)^2 - (x_k^Q G_d)^2\right]. \end{aligned} \tag{15}$$

To understand the effects of I/Q imbalance on the accumulated noise at each receiver antenna, it would be useful to consider a special case where the AWGN is PGN. In this case, $\sigma_{\tilde{n}_l^I}^2$, $\sigma_{\tilde{n}_l^I}^2$, and $\mathbb{E}\{\tilde{n}_l{}^I \tilde{n}_l{}^Q\}$ are given by

$$\begin{aligned} \sigma_{\tilde{n}_l^I}^2 &= \frac{\sigma_n^2}{2} + E\frac{\sigma_e^2}{2}\left[(x_k^I - x_k^Q G_c)^2 + (x_k^Q G_d)^2\right], \\ \sigma_{\tilde{n}_l^Q}^2 &= (K_c^2 + K_d^2)\left\{\frac{\sigma_n^2}{2} + E\frac{\sigma_e^2}{2}\left[(x_k^I - x_k^Q G_c)^2 + (x_k^Q G_d)^2\right]\right\}, \\ \mathbb{E}\{\tilde{n}_l{}^I \tilde{n}_l{}^Q\} &= K_c\left\{\frac{\sigma_n^2}{2} + E\frac{\sigma_e^2}{2}\left[(x_k^I - x_k^Q G_c)^2 + (x_k^Q G_d)^2\right]\right\}. \end{aligned} \tag{16}$$

Remark: As can be noted from the previous equations, the resulting accumulated noise is improper even though the AWGN is proper. This implies that the traditional ML detector, which ignores the fact that the accumulated noise is improper, cannot work efficiently. There is a consequent need to design an optimal receiver that can address this issue.

On the other hand, the useful signal part of (9) along with the I/Q imbalance effects and fading characteristics are given by

$$\begin{aligned} \tilde{\boldsymbol{\eta}}_p &= \{\tilde{\boldsymbol{h}}_{l,i}^I(x_k^I - x_k^Q G_c) - \tilde{\boldsymbol{h}}_{l,q}^Q x_k^Q G_d\} \\ &+ j\{\tilde{\boldsymbol{h}}_{l,i}^I(x_k^I - x_k^Q G_c)K_c + \tilde{\boldsymbol{h}}_{l,i}^Q(x_k^I - x_k^Q G_c)K_d \\ &- \tilde{\boldsymbol{h}}_{l,q}^Q x_k^Q G_d K_c + \tilde{\boldsymbol{h}}_{l,q}^I x_k^Q G_d K_d\}, \end{aligned} \tag{17}$$

where $p \in \{1, \ldots, N_t^2 M\}$. Considering the received useful signal component vector $\tilde{\boldsymbol{\eta}}_p$ and the complex IGN vector $\tilde{\boldsymbol{n}}$, (9) can be rewritten as

$$\boldsymbol{y} = \sqrt{E}\tilde{\boldsymbol{\eta}}_p + \tilde{\boldsymbol{n}}. \tag{18}$$

IV. OPTIMAL ML RECEIVER DESIGN

It was shown in the previous section that the accumulative noise at the receiver is improper. In this section, an optimal ML detector is proposed for the presented QSM wireless communication system operating under this practical constraint.

Considering the general signal model in (18), the joint multivariate probability density function (PDF) of the real part, $\boldsymbol{y}^I$, and the imaginary part, $\boldsymbol{y}^Q$, of the received signal can be derived, such that the I/Q imbalance parameters are known at the receiver side, as

$$f_{\boldsymbol{Y}^I,\boldsymbol{Y}^Q}(\boldsymbol{y}^I, \boldsymbol{y}^Q|\tilde{\boldsymbol{\eta}}_p) = \left(\frac{1}{2\pi\sigma_{\tilde{n}_l^I}\sigma_{\tilde{n}_l^Q}\sqrt{1-\varrho_l^2}}\right)^{N_r} \times \exp\left(\frac{-1}{2(1-\varrho_l^2)}\left[\frac{\|\boldsymbol{y}^I - \sqrt{E}\tilde{\boldsymbol{\eta}}_p^I\|^2}{\sigma_{\tilde{n}_l^I}^2} + \frac{\|\boldsymbol{y}^Q - \sqrt{E}\tilde{\boldsymbol{\eta}}_p^Q\|^2}{\sigma_{\tilde{n}_l^Q}^2} - \frac{2\varrho_l(\boldsymbol{y}^I - \sqrt{E}\tilde{\boldsymbol{\eta}}_p^I)^T(\boldsymbol{y}^Q - \sqrt{E}\tilde{\boldsymbol{\eta}}_p^Q)}{\sigma_{\tilde{n}_l^I}\sigma_{\tilde{n}_l^Q}}\right]\right). \tag{19}$$

The optimal ML detector is designed by maximizing the following conditional probability for equiprobable symbols

$$\hat{p} = \arg\max_p \{f_{\boldsymbol{y}^I,\boldsymbol{y}^Q}(\boldsymbol{y}^I, \boldsymbol{y}^Q|\tilde{\boldsymbol{\eta}}_p)\}. \tag{20}$$

Using (19) and (20), a decision rule for an optimal ML, which jointly accounts for the errors in transmitter indices and symbol detection, can be defined by

$$\hat{p} = \arg\min_p \left\{\frac{\|\boldsymbol{y}^I - \sqrt{E}\tilde{\boldsymbol{\eta}}_p^I\|^2}{\sigma_{\tilde{n}_l^I}^2} + \frac{\|\boldsymbol{y}^Q - \sqrt{E}\tilde{\boldsymbol{\eta}}_p^Q\|^2}{\sigma_{\tilde{n}_l^Q}^2} - \frac{2\varrho_l(\boldsymbol{y}^I - \sqrt{E}\tilde{\boldsymbol{\eta}}_p^I)^T(\boldsymbol{y}^Q - \sqrt{E}\tilde{\boldsymbol{\eta}}_p^Q)}{\sigma_{\tilde{n}_l^I}\sigma_{\tilde{n}_l^Q}}\right\}. \tag{21}$$

The traditional (blind) ML detector, which neglects the improper characteristics of the accumulative noise and ignores the I/Q imbalance effects under ideal hardware assumptions, cannot provide an optimal solution for our system model as we need to consider the amplitude imbalance (ξ_t and ξ_r) and the phase impairment (β_t and β_r). In the case of traditional ML detection, a non-optimal detector can be given by assuming that $\tilde{\boldsymbol{\eta}}_p$, which is under the effects of I/Q imbalance, was sent and G_1, G_2, K_1 and K_2 are unknown at the receiver side

$$[\hat{i}, \hat{q}, \hat{x}_k^I, \hat{x}_k^Q] = \arg\min_{i,q,x_k} \|\boldsymbol{y} - \sqrt{E}(\tilde{\boldsymbol{h}}_i x_k^I + j\tilde{\boldsymbol{h}}_q x_k^Q)\|^2. \tag{22}$$

V. PERFORMANCE ANALYSIS

A. AVERAGE PAIRWISE ERROR PROBABILITY

Considering the detection rule in (21), the probability of error detection can be determined from (23). Keeping in mind that $\tilde{\boldsymbol{\eta}}_p$ is transmitted while $\hat{\boldsymbol{\eta}}_p$ is received, the probability of error at the receiver is

$$\Pr\left(\tilde{\boldsymbol{\eta}}_p \to \hat{\boldsymbol{\eta}}_p|\tilde{\boldsymbol{H}}\right) = \Pr\left(\frac{\|\boldsymbol{y}^I - \sqrt{E}\tilde{\boldsymbol{\eta}}_p^I\|^2}{\sigma_{\tilde{n}_l^I}^2} + \frac{\|\boldsymbol{y}^Q - \sqrt{E}\tilde{\boldsymbol{\eta}}_p^Q\|^2}{\sigma_{\tilde{n}_l^Q}^2} - \frac{2\varrho_l(\boldsymbol{y}^I - \sqrt{E}\tilde{\boldsymbol{\eta}}_p^I)^T(\boldsymbol{y}^Q - \sqrt{E}\tilde{\boldsymbol{\eta}}_p^Q)}{\sigma_{\tilde{n}_l^I}\sigma_{\tilde{n}_l^Q}} > \frac{\|\boldsymbol{y}^I - \sqrt{E}\hat{\boldsymbol{\eta}}_p^I\|^2}{\sigma_{\tilde{n}_l^I}^2} + \frac{\|\boldsymbol{y}^Q - \sqrt{E}\hat{\boldsymbol{\eta}}_p^Q\|^2}{\sigma_{\tilde{n}_l^Q}^2} - \frac{2\varrho_l(\boldsymbol{y}^I\sqrt{E}\hat{\boldsymbol{\eta}}_p^I)^T(\boldsymbol{y}^Q - \sqrt{E}\hat{\boldsymbol{\eta}}_p^Q)}{\sigma_{\tilde{n}_l^I}\sigma_{\tilde{n}_l^Q}}\right). \tag{23}$$

Here, $\hat{\boldsymbol{\eta}}_p = \{\hat{\tilde{\boldsymbol{h}}}_{l,i}^I(\hat{x}_k^I - \hat{x}_k^Q G_c) - \hat{\tilde{\boldsymbol{h}}}_{l,q}^Q \hat{x}_k^Q G_d\} + j\{\hat{\tilde{\boldsymbol{h}}}_{l,i}^I(\hat{x}_k^I - \hat{x}_k^Q G_c)K_c + \hat{\tilde{\boldsymbol{h}}}_{l,i}^Q(\hat{x}_k^I - \hat{x}_k^Q G_c)K_d - \hat{\tilde{\boldsymbol{h}}}_{l,q}^Q \hat{x}_k^Q G_d K_c + \hat{\tilde{\boldsymbol{h}}}_{l,q}^I \hat{x}_k^Q G_d K_d\}$, where $\hat{\tilde{\boldsymbol{h}}}_i$ and $\hat{\tilde{\boldsymbol{h}}}_q$ are complex channel coefficients that are related to detected TAs and that transmit the real and imaginary parts of the detected signal $\hat{x}_k$. After doing some mathematical simplifications, it can be determined that

$$\begin{aligned}\text{PEP} = \Pr\Bigg(&\frac{2\varrho_l\sqrt{E}\{(\tilde{\boldsymbol{\eta}}_p^I - \hat{\boldsymbol{\eta}}_p^I)^T\tilde{\boldsymbol{n}}_l^Q(\tilde{\boldsymbol{\eta}}_p^Q - \hat{\boldsymbol{\eta}}_p^Q)^T\tilde{\boldsymbol{n}}_l^I\}}{\sigma_{\tilde{n}_l^I}\sigma_{\tilde{n}_l^Q}} - \\ &\frac{2\sqrt{E}(\tilde{\boldsymbol{\eta}}_p^I - \hat{\boldsymbol{\eta}}_p^I)^T\tilde{\boldsymbol{n}}_l^I}{\sigma_{\tilde{n}_l^I}^2} - \frac{2\sqrt{E}(\tilde{\boldsymbol{\eta}}_p^Q - \hat{\boldsymbol{\eta}}_p^Q)^T\tilde{\boldsymbol{n}}_l^Q}{\sigma_{\tilde{n}_l^Q}^2} - \frac{E\|\tilde{\boldsymbol{\eta}}_p^I - \hat{\boldsymbol{\eta}}_p^I\|^2}{\sigma_{\tilde{n}_l^I}^2} \\ &- \frac{E\|\tilde{\boldsymbol{\eta}}_p^Q - \hat{\boldsymbol{\eta}}_p^Q\|^2}{\sigma_{\tilde{n}_l^Q}^2} + \frac{2\varrho_l E\left(\tilde{\boldsymbol{\eta}}_p^I - \hat{\boldsymbol{\eta}}_p^I\right)^T(\tilde{\boldsymbol{\eta}}_p^Q - \hat{\boldsymbol{\eta}}_p^Q)}{\sigma_{\tilde{n}_l^I}\sigma_{\tilde{n}_l^Q}} > 0\Bigg) \\ = \Pr(\mathcal{K} > 0),\end{aligned} \tag{24}$$

where $\mathcal{K}$ is a Gaussian RV. The mean and variance of $\mathcal{K}$ are obtained respectively as

$$\mu_{\mathcal{K}} = E\left(\frac{\|\tilde{\boldsymbol{\eta}}_p^I - \hat{\boldsymbol{\eta}}_p^I\|^2}{\sigma_{\tilde{n}_l^I}^2} + \frac{\|\tilde{\boldsymbol{\eta}}_p^Q - \hat{\boldsymbol{\eta}}_p^Q\|^2}{\sigma_{\tilde{n}_l^Q}^2} - \frac{2\varrho_l\left(\tilde{\boldsymbol{\eta}}_p^I - \hat{\boldsymbol{\eta}}_p^I\right)^T(\tilde{\boldsymbol{\eta}}_p^Q - \hat{\boldsymbol{\eta}}_p^Q)}{\sigma_{\tilde{n}_l^I}\sigma_{\tilde{n}_l^Q}}\right). \tag{25}$$

$$\sigma_{\mathcal{K}}^2 = 4E(1-\varrho_l^2)\times \left(\frac{\|\tilde{\boldsymbol{\eta}}_p^I - \hat{\boldsymbol{\eta}}_p^I\|^2}{\sigma_{\tilde{n}_l^I}^2} + \frac{\|\tilde{\boldsymbol{\eta}}_p^Q - \hat{\boldsymbol{\eta}}_p^Q\|^2}{\sigma_{\tilde{n}_l^Q}^2} - \frac{2\varrho_l\left(\tilde{\boldsymbol{\eta}}_p^I - \hat{\boldsymbol{\eta}}_p^I\right)^T(\tilde{\boldsymbol{\eta}}_p^Q - \hat{\boldsymbol{\eta}}_p^Q)}{\sigma_{\tilde{n}_l^I}\sigma_{\tilde{n}_l^Q}}\right). \tag{26}$$

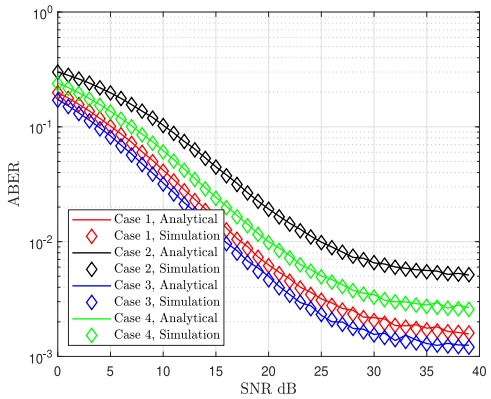

FIGURE 2. APEP of QSM system over Beckmann channels conditions with imperfect CSI, IGN, and I/Q impaired transmitter and receiver.

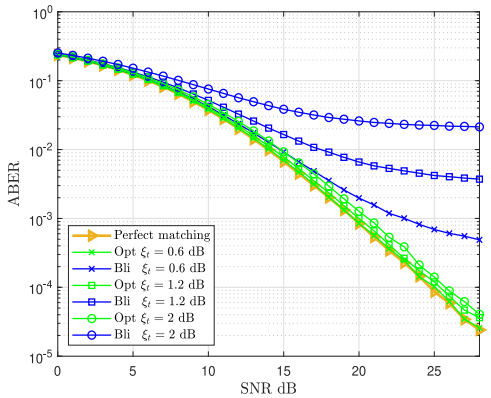

FIGURE 3. 2 × 2 QSM MIMO system with 4-QAM modulation in the presence of different levels of amplitude imbalance at the transmitter side with fixed $\beta_t = 5°$.

Now, from (25) and (26), PEP can be given as

$$\text{PEP} = Q\left(\frac{\mu_{\mathcal{K}}}{\sqrt{\sigma^2_{\mathcal{K}}}}\right) = Q\left(\sqrt{E_s\boldsymbol{\zeta}}\right), \tag{27}$$

where $\boldsymbol{\zeta} = \left(\frac{\|\tilde{\boldsymbol{\eta}}_p^I - \hat{\boldsymbol{\eta}}_p^I\|^2}{\sigma^2_{\tilde{n}_l^I}} + \frac{\|\tilde{\boldsymbol{\eta}}_p^Q - \hat{\boldsymbol{\eta}}_p^Q\|^2}{\sigma^2_{\tilde{n}_l^Q}} - \frac{2\varrho_l(\tilde{\boldsymbol{\eta}}_p^I - \hat{\boldsymbol{\eta}}_p^I)^T(\tilde{\boldsymbol{\eta}}_p^Q - \hat{\boldsymbol{\eta}}_p^Q)}{\sigma_{\tilde{n}_l^I}\sigma_{\tilde{n}_l^Q}}\right)$ and $E_s = \frac{E}{4(1-\varrho_l^2)}$. Based on this expression, it can be said that PEP mainly depends on the Euclidean distance between the transmitted and detected signal components, the I/Q imbalance distortions, the energy of the signal, and the variance of the estimation error.

Now, the average pairwise error probability (APEP) can be determined by using the expected value of PEP from (27) as

$$\text{APEP} = \mathbb{E}\left\{Q\left(\sqrt{E_s\boldsymbol{\zeta}}\right)\right\} = \int_{-\infty}^{\infty} Q\left(\sqrt{E_s\boldsymbol{\zeta}}\right) f_\zeta(\zeta)d\zeta. \tag{28}$$

It is difficult to determine the PDF of $\boldsymbol{\zeta}$ (i.e., $f_\zeta(\zeta)$) in this expression since it uses a Beckmann fading channel model. This can be solved by noting that ζ can be written in matrix form as $\zeta = \mathbf{x}^T\mathbf{A}\mathbf{x}$. Here $\mathbf{x} \sim \mathcal{N}(\boldsymbol{\mu_x}, \boldsymbol{\sigma_x^2})$ where $\mathbf{x}^T = [x_1 \;\; x_2]$, $x_1 = (\tilde{\boldsymbol{\eta}}_p^I - \hat{\boldsymbol{\eta}}_p^I)$, $x_2 = (\tilde{\boldsymbol{\eta}}_p^Q - \hat{\boldsymbol{\eta}}_p^Q)$, and $\mathbf{A}$ is the quadratic matrix. Assuming, without loss of generality, that the indices $\hat{i} \neq q$ and $\hat{q} \neq i$, the parameters of x_1 and x_2 can be given by

$$\begin{aligned}\mu_{x_1} &= k_c\mu^I_{\hat{h}}(\tilde{x}_k^I - \hat{\tilde{x}}_k^I) + k_d\mu^Q_{\hat{h}}(\tilde{x}_k^I - \hat{\tilde{x}}_k^I)\\ &\quad - k_c\mu^Q_{\hat{h}}(\tilde{x}_k^Q - \hat{\tilde{x}}_k^Q) + k_d\mu^I_{\hat{h}}(\tilde{x}_k^Q - \hat{\tilde{x}}_k^Q),\\ \mu_{x_2} &= \mu^I_{\hat{h}}(\tilde{x}_k^I - \hat{\tilde{x}}_k^I) - \mu^Q_{\hat{h}}(\tilde{x}_k^Q - \hat{\tilde{x}}_k^Q).\end{aligned} \tag{29}$$

$$\sigma^2_{x_1} = \begin{cases}(i \neq \hat{i}, q \neq \hat{q})\\ K_c^2\sigma^2_{\hat{h}^I}[(\tilde{x}_k^I)^2 + (\hat{\tilde{x}}_k^I)^2] + K_d^2\sigma^2_{\hat{h}^Q}[(\tilde{x}_k^I)^2 + (\hat{\tilde{x}}_k^I)^2]\\ +4\rho_{\hat{h}}K_cK_d\sigma^I_{\hat{h}}\sigma^Q_{\hat{h}}[(\tilde{x}_k^I)^2 + (\hat{\tilde{x}}_k^I)^2]\\ +K_d^2\sigma^2_{\hat{h}^I}[(\tilde{x}_k^Q)^2 + (\hat{\tilde{x}}_k^Q)^2] + K_c^2\sigma^2_{\hat{h}^Q}[(\tilde{x}_k^Q)^2\\ +(\hat{\tilde{x}}_k^Q)^2]\\ -4\rho_{\hat{h}}K_cK_d\sigma^I_{\hat{h}}\sigma^Q_{\hat{h}}[(\tilde{x}_k^Q)^2 + (\hat{\tilde{x}}_k^Q)^2]\\ \\ (i = \hat{i}, q \neq \hat{q})\\ K_c^2\sigma^2_{\hat{h}^I}[(\tilde{x}_k^I - \hat{\tilde{x}}_k^I)^2] + K_d^2\sigma^2_{\hat{h}^Q}[(\tilde{x}_k^I - \hat{\tilde{x}}_k^I)^2]\\ +2\rho_{\hat{h}}K_cK_d\sigma^I_{\hat{h}}\sigma^Q_{\hat{h}}[(\tilde{x}_k^I - \hat{\tilde{x}}_k^I)^2]\\ +K_d^2\sigma^2_{\hat{h}^I}[(\tilde{x}_k^Q)^2 + (\hat{\tilde{x}}_k^Q)^2] + K_c^2\sigma^2_{\hat{h}^Q}[(\tilde{x}_k^Q)^2\\ +(\hat{\tilde{x}}_k^Q)^2]\\ -4\rho_{\hat{h}}K_cK_d\sigma^I_{\hat{h}}\sigma^Q_{\hat{h}}[(\tilde{x}_k^Q)^2 + (\hat{\tilde{x}}_k^Q)^2]\\ \\ (i \neq \hat{i}, q = \hat{q})\\ K_c^2\sigma^2_{\hat{h}^I}[(\tilde{x}_k^I)^2 + (\hat{\tilde{x}}_k^I)^2] + K_d^2\sigma^2_{\hat{h}^Q}[(\tilde{x}_k^I)^2 + (\hat{\tilde{x}}_k^I)^2]\\ +4\rho_{\hat{h}}K_cK_d\sigma^I_{\hat{h}}\sigma^Q_{\hat{h}}[(\tilde{x}_k^I)^2 + (\hat{\tilde{x}}_k^I)^2]\\ +K_d^2\sigma^2_{\hat{h}^I}[(\tilde{x}_k^Q - \hat{\tilde{x}}_k^Q)^2] + K_c^2\sigma^2_{\hat{h}^Q}[(\tilde{x}_k^Q - \hat{\tilde{x}}_k^Q)^2]\\ -2\rho_{\hat{h}}K_cK_d\sigma^I_{\hat{h}}\sigma^Q_{\hat{h}}[(\tilde{x}_k^Q - \hat{\tilde{x}}_k^Q)^2]\\ \\ (i = \hat{i}, q = \hat{q})\\ K_c^2\sigma^2_{\hat{h}^I}[(\tilde{x}_k^I - \hat{\tilde{x}}_k^I)^2] + K_d^2\sigma^2_{\hat{h}^Q}[(x_k^I - \hat{\tilde{x}}_k^I)^2]\\ +2\rho_{\hat{h}}K_cK_d\sigma^I_{\hat{h}}\sigma^Q_{\hat{h}}[(x_k^I - \hat{\tilde{x}}_k^I)^2]\\ +K_d^2\sigma^2_{\hat{h}^I}[(\tilde{x}_k^Q - \hat{\tilde{x}}_k^Q)^2] + K_c^2\sigma^2_{\hat{h}^Q}[(\tilde{x}_k^Q - \hat{\tilde{x}}_k^Q)^2]\\ -2\rho_{\hat{h}}K_cK_d\sigma^I_{\hat{h}}\sigma^Q_{\hat{h}}[(\tilde{x}_k^Q - \hat{\tilde{x}}_k^Q)^2].\end{cases} \tag{30}$$

$$\sigma^2_{x_2} = \begin{cases}(i \neq \hat{i}, q \neq \hat{q})\\ \sigma^2_{\hat{h}^I}[(\tilde{x}_k^I)^2 + (\hat{\tilde{x}}_k^I)^2] + \sigma^2_{\hat{h}^Q}[(\tilde{x}_k^Q)^2 + (\hat{\tilde{x}}_k^Q)^2]\\ \\ (i = \hat{i}, q \neq \hat{q})\\ \sigma^2_{\hat{h}^I}[(\tilde{x}_k^I - \hat{\tilde{x}}_k^I)^2] + \sigma^2_{\hat{h}^Q}[(\tilde{x}_k^Q)^2 + (\hat{\tilde{x}}_k^Q)^2]\\ \\ (i \neq \hat{i}, q = \hat{q})\\ \sigma^2_{\hat{h}^I}[(\tilde{x}_k^I)^2 + (\hat{\tilde{x}}_k^I)^2] + \sigma^2_{\hat{h}^Q}[(\tilde{x}_k^Q - \hat{\tilde{x}}_k^Q)^2]\\ \\ (i = \hat{i}, q = \hat{q})\\ \sigma^2_{\hat{h}^I}[(\tilde{x}_k^I - \hat{\tilde{x}}_k^I)^2] + \sigma^2_{\hat{h}^Q}[(\tilde{x}_k^Q - \hat{\tilde{x}}_k^Q)^2].\end{cases} \tag{31}$$

$$\mathbb{E}\{x_1x_2\} = \begin{cases} (i \neq \hat{i}, q \neq \hat{q}) \\ K_c\sigma^2_{\hat{h}^I}[(\tilde{x}^I_k)^2 + (\hat{\tilde{x}}^I_k)^2] + K_c\sigma^2_{\hat{h}^Q}[(\tilde{x}^Q_k)^2 + (\hat{\tilde{x}}^Q_k)^2] \\ +K_d\rho_{\hat{h}}\sigma^I_{\hat{h}}\sigma^Q_{\hat{h}}[(\tilde{x}^I_k)^2 + (\hat{\tilde{x}}^I_k)^2 - (\tilde{x}^Q_k)^2 - (\hat{\tilde{x}}^Q_k)^2] \\ \\ (i = \hat{i}, q \neq \hat{q}) \\ K_c\sigma^2_{\hat{h}^I}[(\tilde{x}^I_k - \hat{\tilde{x}}^I_k)^2] + K_c\sigma^2_{\hat{h}^Q}[(\tilde{x}^Q_k)^2 + (\hat{\tilde{x}}^Q_k)^2] \\ +K_d\rho_{\hat{h}}\sigma^I_{\hat{h}}\sigma^Q_{\hat{h}}[(\tilde{x}^I_k - \hat{\tilde{x}}^I_k)^2 - (\tilde{x}^Q_k)^2 + (\hat{\tilde{x}}^Q_k)^2] \\ \\ (i \neq \hat{i}, q = \hat{q}) \\ K_c\sigma^2_{\hat{h}^I}[(\tilde{x}^I_k)^2 \\ +(\hat{\tilde{x}}^I_k)^2] + K_d\rho_{\hat{h}}\sigma^I_{\hat{h}}\sigma^Q_{\hat{h}}[(\tilde{x}^I_k)^2 + (\hat{\tilde{x}}^I_k)^2] \\ +K_c\sigma^2_{\hat{h}^Q}[(\tilde{x}^Q_k - \hat{\tilde{x}}^Q_k)^2] \\ -\rho_{\hat{h}}K_cK_d\sigma^I_{\hat{h}}\sigma^Q_{\hat{h}}[(\tilde{x}^Q_k - \hat{\tilde{x}}^Q_k)^2] \\ \\ (i = \hat{i}, q = \hat{q}) \\ K_c\sigma^2_{\hat{h}^I}[(\tilde{x}^I_k - \hat{\tilde{x}}^I_k)^2] + K_d\rho_{\hat{h}}\sigma^I_{\hat{h}}\sigma^Q_{\hat{h}}[(\tilde{x}^I_k - \hat{\tilde{x}}^I_k)^2] \\ +K_c\sigma^2_{\hat{h}^Q}[(\tilde{x}^Q_k - \hat{\tilde{x}}^Q_k)^2] \\ -\rho_{\hat{h}}K_cK_d\sigma^I_{\hat{h}}\sigma^Q_{\hat{h}}[(\tilde{x}^Q_k - \hat{\tilde{x}}^Q_k)^2]. \end{cases} \tag{32}$$

$$\rho_x = \frac{\mathbb{E}\{x_1x_2\} - \mu_{x_1}\mu_{x_2}}{(\sigma_{x_1}\sigma_{x_2})}. \tag{33}$$

Hence, in a quadratic form, ζ has the PDF of two correlated noncentral chi-squared RVs. From Appendix A, the moment generating function (MGF) of ζ can be given by

$$M_\zeta(t) = \left(\frac{\exp\left(\frac{a_1^2\Lambda_1 t}{1-2\Lambda_1 t} + \frac{a_2^2\Lambda_2 t}{1-2\Lambda_2 t} \right)}{\sqrt{1-2(\Lambda_1+\Lambda_2)t + 4\Lambda_1\Lambda_2 t^2}} \right)^{N_r}, \tag{34}$$

where the eigenvalues Λ_1 and Λ_2, and the mean values b_1 and b_2 are calculated as in Appendix A. In addition, this Appendix shows how other channel models can be considered as special cases of the Beckmann fading model. For example, (34) can be used in the case of Rayleigh fading channels. Then, $\mu_{x1} = \mu_{x2} = 0$, $\sigma^2_{x_1} = \sigma^2_{x_2}$, and $\rho_x = 0$. Relaxing the condition $\mu_{x1} = \mu_{x2} = 0$ to give the line of sight (LoS) competent $\mu_{x1} = \mu_{x2}$ gives the Rician fading channels. In light of this information, an exact expression for the APEP can be formulated by using (27)-(34) as

$$\text{APEP} = \frac{1}{\pi}\int_0^{\frac{\pi}{2}} M_\zeta\left(-\frac{E_s}{2\sin^2\Theta}\right)d\Theta. \tag{35}$$

B. ASYMPTOTIC ANALYSIS

Even though the exact expression of APEP given in (35) provides a numerical evaluation of the system performance, it does not present the effects of key parameters on the system's behavior. Hence, assuming that $E_s >> 1$, an asymptotic APEP can be introduced by using (34) and (35) as

$$\text{APEP}_{\text{asy}} = \frac{1}{\pi}\left(\frac{\exp(-\frac{a_1^2+a_2^2}{2})}{(E_s/\sigma^2_{\tilde{n}^I_l})\sqrt{1-\varrho_l^2}} \right)^{N_r} \int_0^{\frac{\pi}{2}} (\sin\Theta)^{2N_r} d\Theta. \tag{36}$$

In this case, considering that $\int_0^{\frac{\pi}{2}} (\sin\Theta)^{2N_r} d\Theta = \frac{\sqrt{\pi}\,\Gamma(N_r+\frac{1}{2})}{2\Gamma(N_r+1)}$, where $\Gamma(\cdot)$ is the gamma function, and applying some mathematical operations, APEP_{asy} may be simplified to

$$\text{APEP}_{\text{asy}} = \frac{(2N_r-1)!!}{2^{N_r+1}N_r!}\left(\frac{\exp\left(-\frac{a_1^2+a_2^2}{2}\right)}{\sqrt{1-\varrho_l^2}} \right)^{N_r} (E_s/\sigma^2_{\tilde{n}^I_l})^{-N_r}. \tag{37}$$

It is clear from (37) that the APEP depends on the number of receiver antennas, the average value of the received signal, the energy of the transmitted signal as well as the variance of the noise. In addition, the diversity gain is equal to the number of receiver antennas, as in the case of perfect I/Q balance, and can be found by using

$$\text{Diversity gain} = -\lim_{\text{SNR}\to\infty} \frac{\log(\text{APEP}_{\text{asy}})}{\log(\text{SNR})} = N_r. \tag{38}$$

Finally, the ABER can be upper-bound as [41],

$$\text{ABER}_{\text{QSM}} \leq \frac{1}{2^{\tilde{m}}}\sum_{p=1}^{2^{\tilde{m}}}\sum_{q=1}^{2^{\tilde{m}}} \frac{1}{\tilde{m}}\Pr\left(\tilde{\eta}_p \to \hat{\eta}_p\right)\Omega_{p,q}, \tag{39}$$

where $\tilde{m} = \log_2(N_T^2 M)$ is the number of bits transmitted in active antenna indices and modulated symbols while $\Omega_{p,q}$ is the number of bits in error related to the relevant pairwise error event.

VI. NUMERICAL ANALYSIS AND RESULTS

In this section, the effects of I/Q imbalance at the transmitter and receiver, imperfect CSI, IGN, fading channel model, diversity gain, and modulation order on the performance of the QSM wireless communication system are studied and analyzed. Considering the aforementioned QSM receiver design, Monte Carlo simulations were executed to validate the theoretical results and evaluate the system performance. Unless otherwise specified, the 4-QAM technique is used and the computer simulations are performed assuming Rayleigh fading channels. The noise at the receiver is PGN with zero mean and $\sigma_n^2 = 1$ variance. Moreover, the energy of the transmitted signal is normalized by $(|x_iG_1 + x_i^*G_2|^2)$ to guarantee a fair comparison. All results are compared to a system with perfect I/Q balance. In addition, all computer simulations were realized using at least 10^6 symbols transmitted for each signal-to-noise ratio (SNR) value. Fig. 2 shows the simulation and analytical results where the APEP values of the optimal receiver were calculated using (34) and (35). The simulation parameters consisted of $\mu_{h^I} = .001$, $\mu_{h^Q} = .05$, $\sigma^2_{h^I} = 0.4$, $\sigma^2_{h^Q} = 0.6$, $\rho_h = -0.3$, $\sigma^2_{n^I} = 0.7$, $\sigma^2_{n^Q} = 0.3$, $\rho_n = 0.3$ $\sigma^2_{e^I} = 0.001$, $\sigma^2_{e^Q} = 0.002$, $\rho_e = 0.3$, $\xi_{t,r} = -1.5$ dB, and $\beta_{t,r} = 5^\circ$.

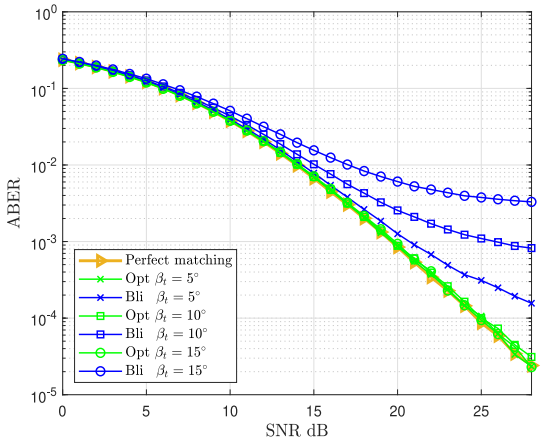

FIGURE 4. 2 × 2 QSM MIMO system with 4-QAM modulation in the presence of different levels of angle mismatches at the transmitter side with fixed ξ_t=0.3 dB.

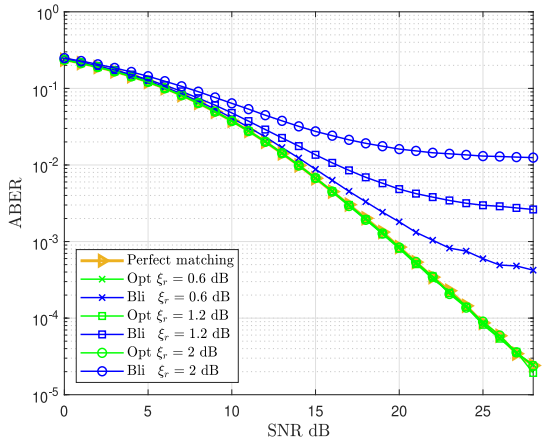

FIGURE 5. 2 × 2 QSM MIMO system with 4-QAM modulation in the presence of different levels of amplitude imbalance at the receiver side with fixed $\beta_r = 5°$.

These parameters were chosen using a general fading channel model (i.e., the Beckmann model) with imperfect CSI, general Gaussian noise conditions (IGN), and I/Q impaired transmitter and receiver. Four cases were considered that match the four transmitted and detected channel index possibilities in (30)-(31). It is clear that the simulation results match the analytical ones in all cases, therefore validating our analysis.

Figs. 3 and 4 show the performance of a 2 × 2 QSM system affected by I/Q imbalance at the transmitter side only, with perfect CSI and PGN at the receiver side. Fig. 3 shows the results when the phase mismatch 5° while changing the amplitude imbalance between 0.6, 1.2, and 2 dB. Although I/Q imbalance has only a minor impact on the optimal receiver, this impact is very dramatic in the case of the blind one. In addition, in the higher SNR region, the blind receiver's performance saturates, leading to an error floor and zero power gain. In Fig. 4, the ABER is plotted by fixing the amplitude mismatch at 0.3 dB the phase imbalance is incremented along 5°, 10°, and 15°. It shows that the optimal receiver can eliminate the effects of phase mismatching at the transmitter side. In addition, as in the case of amplitude imbalance, the blind system performance saturates in the high SNR region, leading also to an error floor and zero power gain. Figs. 5 and 6 show the performance of 2 × 2 QSM system affected by I/Q imbalance at the receiver side only, assuming perfect CSI and PGN. Fig. 5 shows the results when the phase mismatch is fixed at 5° at the amplitude imbalance is incremented along 0.6, 1.2, and 2 dB. Fig. 6 illustrates the results of fixing the amplitude mismatch to 0.3 dB while changing the phase imbalance between 5°, 10° and 15°. It can be seen from these figures that the optimal receiver outperforms the blind one and can eliminate the amplitude and phase mismatching effects completely.

Finally, the blind receiver has an very inferior performance at high values of amplitude or phase mismatching. This can be noticed in the higher SNR regions of both figures, where

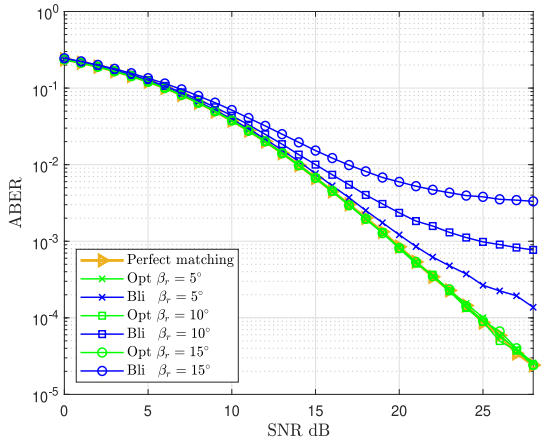

FIGURE 6. 2 × 2 QSM MIMO system with 4-QAM modulation in the presence of different levels of angle mismatches at the receiver side with fixed ξ_r=0.3 dB.

the performance saturates, leading to an error floor and zero power gain. From Figs. 3-6, phase imbalance at the transmitter and receiver sides have almost the same impact on the QSM system when using 4-QAM modulation. However, it is the amplitude imbalance that has more of an effect at the transmitter side.

Figs. 7 and 8 illustrate two QSM configurations. The first uses a 2 × 2 MIMO system with 16-QAM modulation, achieving an SE of 6 bps/Hz. A similar SE is also obtained with a 4 × 2 MIMO system using 4-QAM modulation. The results in these figures have patterns similar to those of the previous figures and confirm the superiority of the proposed receiver. The remarkable finding here is that the effects of I/Q imbalance are more critical in the case of 2 × 2 even though the receivers in both figures achieve the same spectral efficiencies. This presents as a 1 dB gain difference in the optimal receiver performance at 10^{-3} ABER when $\xi_{t,r} = 1$ dB.

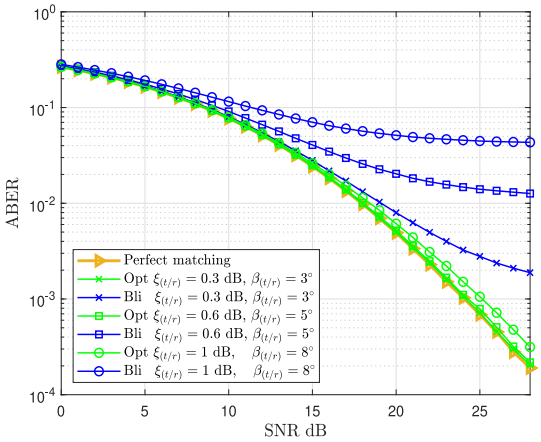

FIGURE 7. 2 × 2 QSM MIMO system with 16-QAM modulation in the presence of different levels of I/Q imbalance.

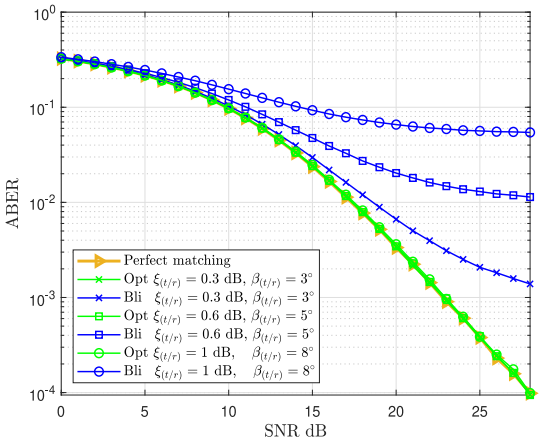

FIGURE 8. 4 × 2 QSM MIMO system with 4-QAM modulation in the presence of different levels of I/Q imbalance.

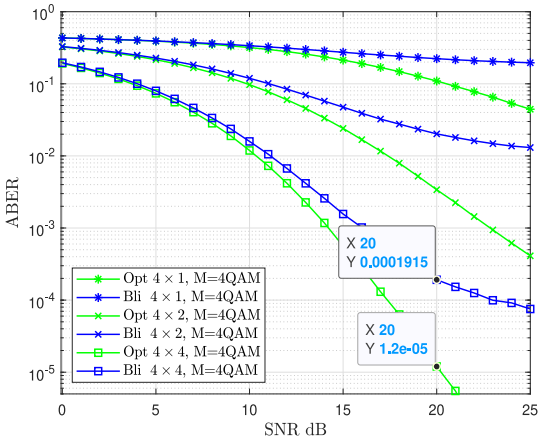

FIGURE 9. 4 × 1, 4 × 2, and 4 × 4 QSM MIMO systems with 4-QAM modulation when $\xi_{t,r}$=0.3 dB and $\beta_{t,r}$ =5°.

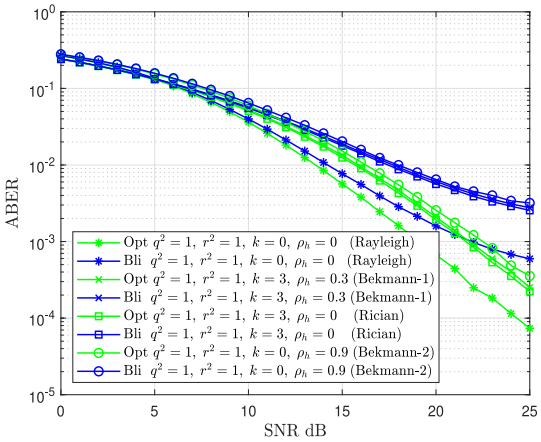

FIGURE 10. ABER performance of 2 × 2 QSM system over Beckmann channels when $\xi_{t,r}$=0.3 dB and $\beta_{t,r}$ =5°.

Fig. 9 illustrates the ABER performance of 4 × 1, 4 × 2, and 4 × 4 QSM MIMO systems with 4-QAM modulation in the presence of $\xi_{t,r}$=0.3 dB and $\beta_{t,r}$ =5° I/Q imbalance parameters. As this figure shows, the diversity order in the case of the optimal receiver is N_r, and increasing the SNR enhances the system's performance. This gain can be seen where the ABER results at high SNR have gains of 1, 2, and 3 for Nr=1, Nr=2, and Nr=3, respectively. On the other hand, increasing the SNR has no impact on the ABER in the case of the blind receiver, ultimately leading to an error floor and a diversity order of zero.

Fig. 10 shows the effects of the channel parameters outlines in Section B. To guarantee a fair comparison, $\Omega = 1$ for all channels. $\Omega = \mu_{h^I}^2 + \mu_{h^Q}^2 + \sigma_{h^I}^2 + \sigma_{h^Q}^2$, and indicates the average power of the fading channel. As the figure shows, the channel parameters have the same effects on both receivers. Here, Rician Beckmann-1 fading channels demonstrate poor performance compared to the Rayleigh channel, and this occurs because they have a minimum variance. Even more, the QSM system relies heavily on the difference in the channel conditions when transmitting the spatial bits. Here, the parameter K indicates the ratio between the LoS and non-LoS power. There is about a 5 dB difference at 10^{-3} ABER in the power gain between the Rayleigh channel and the Beckmann-2 channel, where the latter uses the same Rayleigh parameters other than having correlated I and Q components. On the other hand, the correlation has less of an effect when there is a strong LoS channel path. This can be seen when noting the same error performance in the Beckmann channel-1, which has the same Rician parameters save for correlated I and Q components.

Fig. 11 illustrates the performance of a 2 × 2 QSM MIMO system under the effects of different levels of imperfect CSI for $\xi_{t,r} = 0.3$ dB and $\beta_{t,r} = 5°$. This figure shows that the imperfect CSI has a significant impact on both receivers, where the performance saturates in the high SNR region, leading to an error floor and zero power gain. Comparing the results here with the previous one shows that small values of σ_e^2

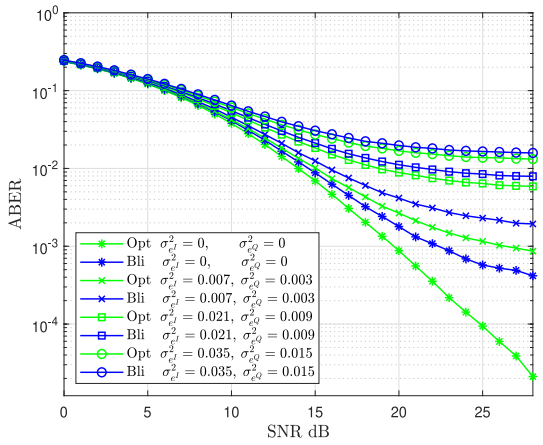

FIGURE 11. ABER performance of 2 × 2 QSM with different levels of improper channel estimation errors when $\xi_{t,r}$=0.3 dB and $\beta_{t,r}$ =5°.

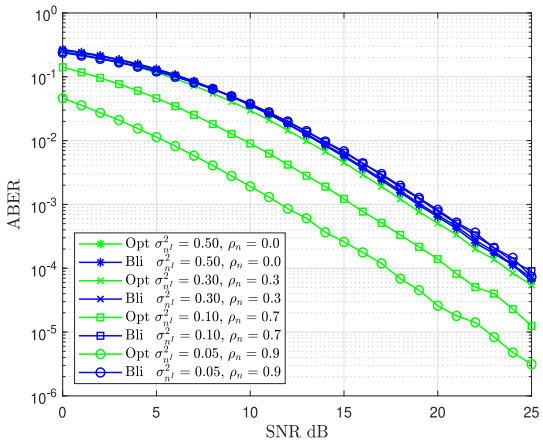

FIGURE 12. ABER performance of 2 × 2 QSM with different levels of IGN assuming that $\sigma_I^2+\sigma_Q^2$=1.

has a considerable effect on the performance of the optimal receiver, and its performance worsens to that of the blind one at higher values of σ_e^2.

Fig. 12 shows the effect of IGN on a 2 × 2 QSM MIMO system. Here, the I/Q components match perfectly. The results in this figure can be interpreted from (27), where the term inside the Q-function approaches ∞ and the error probability approaches zero in two scenarios: *scenario* 1, when one of the variances $\sigma_{n_Q}^2$ or $\sigma_{n_I}^2$ goes to zero because then the numerator goes to ∞. *scenario* 2, when the correlation factor of the AWGN goes to one, because then the denominator goes to zero. This trend is not valid for the blind receiver.

VII. CONCLUSION

The importance of considering the effects of I/Q imbalance, channel estimation errors, and IGN for future QSM wireless communication systems was outlined in this paper. An optimal ML detector design was proposed to render QSM systems robust in the face of the detrimental effects of I/Q imbalance in the presence of IGN and imperfect CSI. The systems' performance were evaluated over Beckmann channels considering different special cases. To obtain fair comparisons, we use the same average power (Ω) for each case. The obtained results demonstrated that the proposed optimal receiver successfully mitigates the effects of I/Q imbalance. In the future, the presented analysis can be extended to address the correlated channel models. Moreover, less complex receivers can be proposed using improper Gaussian signalling to optimize the system performance in the presence of the I/Q imbalance.

APPENDIX A
MGF OF QUADRATIC FORM OF NONCENTRAL CHI-SQUARED DISTRIBUTION

Let $\mathbf{A}$ denote an $n \times n$ symmetric matrix with real entries and let $\mathbf{x}$ denote an $n \times 1$ column vector. The quadratic expression of a correlated Gaussian RVs vector $\mathbf{x} \sim \mathcal{N}(\boldsymbol{\mu}, \boldsymbol{\Sigma})$ is given by

$$Q(\mathbf{x}) = \mathbf{x}^T \mathbf{A}\, \mathbf{x}, \tag{40}$$

where $\boldsymbol{\mu}$ is the mean vector and $\boldsymbol{\Sigma}$ is the positive definite covariance of $\mathbf{x}$, and matrix $\mathbf{A}$ is the quadratic matrix. Assuming $\mathbf{y} = \boldsymbol{\Sigma}^{-\frac{1}{2}}\, \mathbf{x}$, $Q(\mathbf{x})$ can be rewritten as

$$Q(\mathbf{x}) = \mathbf{y}^T \boldsymbol{\Sigma}^{\frac{1}{2}} \mathbf{A} \boldsymbol{\Sigma}^{\frac{1}{2}} \mathbf{y}. \tag{41}$$

Denoting $\boldsymbol{P}$ to be an orthonormal $p \times p$ matrix which diagonalizes $\boldsymbol{\Sigma}^{\frac{1}{2}} \boldsymbol{A} \boldsymbol{\Sigma}^{\frac{1}{2}}$. This means that $\boldsymbol{P}^T \boldsymbol{\Sigma}^{\frac{1}{2}} \boldsymbol{A} \boldsymbol{\Sigma}^{\frac{1}{2}} \boldsymbol{P} = Diag(\Lambda_1, \ldots, \Lambda_p)$. As shown in [42], $Q(\mathbf{x})$ can be rewritten as

$$Q(\mathbf{x}) = \sum_{j=1}^{p} \Lambda_j (U_j + a_j)^2, \tag{42}$$

where $\Lambda_1, \ldots, \Lambda_p$ represents the eigenvalues of $\boldsymbol{\Sigma}^{\frac{1}{2}} \boldsymbol{A} \boldsymbol{\Sigma}^{\frac{1}{2}}$, $a_1, \ldots, b_p = (\boldsymbol{P}^T \boldsymbol{\Sigma}^{-\frac{1}{2}} \boldsymbol{\mu})^T$, and U_j represents independently distributed standard normal RVs. Based on this, $Q(\mathbf{x})$ is distributed as a linear combination of independent noncentral (central if $b_i = 0$) chi-square variables.

The MGF of the quadratic form in (42) can be given in terms of the eigenvalues of $\boldsymbol{\Sigma}^{\frac{1}{2}} \boldsymbol{A} \boldsymbol{\Sigma}^{\frac{1}{2}}$ as in the following equation [42]–[45]

$$M_Q(t) = \prod_{j=1}^{p} \frac{1}{\sqrt{1-2t\Lambda_j}} \exp\left\{ t \sum_{j=1}^{p} \frac{a_j^2 \Lambda_j}{1-2t\Lambda_j} \right\}. \tag{43}$$

If $\boldsymbol{\mu} = \mathbf{0}$, then $Q(\mathbf{x})$ is distributed as a linear combination of independent central chi-square variables. In this case, (43) can be abbreviated to

$$M_Q(t) = \prod_{j=1}^{p} \frac{1}{\sqrt{1-2t\Lambda_j}}. \tag{44}$$

TABLE I The Relation Between Beckmann Fading Model and Other Fading Models in the Literature. The Beckmann Fading Parameters are in Bold

Channels	Beckman Fading Parameters			
One-sided Gaussian	$\boldsymbol{r} = 1,$	$\boldsymbol{q} = 0,$	$\boldsymbol{K} = 0,$	$\boldsymbol{\rho_h} = 0$
Rayleigh	$\boldsymbol{r} = 1,$	$\boldsymbol{q} = 1,$	$\boldsymbol{K} = 0,$	$\boldsymbol{\rho_h} = 0$
Hoyt (Nakagami-q)	$\boldsymbol{r} = 1,$	$\boldsymbol{q} = q,$	$\boldsymbol{K} = 0,$	$\boldsymbol{\rho_h} = 0$
Rician with parameter k	$\boldsymbol{r} = 1,$	$\boldsymbol{q} = 1,$	$\boldsymbol{K} = K,$	$\boldsymbol{\rho_h} = 0$
Another form Rician without LoS	$\boldsymbol{r} = 1,$	$\boldsymbol{q} = 1,$	$\boldsymbol{K} = 0,$	$\boldsymbol{\rho_h} = \rho_h$

APPENDIX B
BECKMANN CHANNELS

The complex fading coefficient h can be expressed in terms of its real and imaginary components as,

$$h = \sum_{i=0}^{L-1} (h_i^I + j h_i^Q) = h^{\mathrm{I}} + j h^{\mathrm{Q}}. \tag{45}$$

Thus, h^{I} and h^{Q}, which are the real and imaginary components of the fading coefficient are derived by assuming a sufficiently large number of random multipath components h_i^I and h_i^Q. This assumption is practical and valid, especially in a rich urban setting which may have a large number of scattering surfaces. Central Limit Theorem states that a normalized RV derived from the sum of a large number of independent identically distributed random components converges to a Gaussian RV. By assuming a sufficiently large number of paths and depending on the Central Limit Theorem [41], the fading channel can be modeled as a complex Gaussian RV.

This topic was originally addressed by Beckmann [46], [47] in its more general form by assuming an arbitrary mean and variance for the real and imaginary parts. h can be modeled as $\mathcal{CN}(\boldsymbol{\mu_h}, \boldsymbol{\sigma_h^2})$ where the mean vector and the covariance matrix of h are given by $\boldsymbol{\mu_h}$ and $\boldsymbol{\sigma_h^2}$ respectively

$$\boldsymbol{\mu_h} = \begin{bmatrix} \mu_{h^I} & \mu_{h^Q} \end{bmatrix}, \boldsymbol{\sigma_h^2} = \begin{bmatrix} \sigma_{h^I}^2 & \rho_h \sigma_h^Q \sigma_h^I \\ \rho_h \sigma_h^Q \sigma_h^I & \sigma_{h^Q}^2 \end{bmatrix}. \tag{46}$$

The joint PDF of the h^{I} and h^{Q} components is given by

$$f_{h^{\mathrm{I}}h^{\mathrm{Q}}}(x,y) = \frac{1}{2\pi\sigma_{h^I}\sigma_{h^Q}\sqrt{1-\rho_h^2}} \times \exp\left\{ -\frac{1}{2(1-\rho^2)} \left[\left(\frac{x-\mu_{h^I}}{\sigma_{h^I}} \right)^2 + \left(\frac{y-\mu_{h^Q}}{\sigma_{h^Q}} \right)^2 - 2\rho_h \frac{(x-\mu_{h^I})(y-\mu_{h^Q})}{\sigma_{h^I}\sigma_{h^Q}} \right] \right\}. \tag{47}$$

Making no assumptions on the statistics of the amplitudes and phases of the fading channel (i.e., allowing h^{I} and h^{Q} to have different means and variances, or being correlated) leads to a more general fading channel model, where most of the well-known fading channel models can be considered as special cases of this general model. For example, when the quadrature components are Gaussian, uncorrelated, zero mean, and equal in variance, this results in the Rayleigh PDF. The Rician PDF is the result when the variances are equal and either one or both components have non-zero mean, whereas the Hoyt PDF assumes zero means and non-equal variances. A form of the Rician distributed envelope also results when the quadrature components are correlated but both of them have zero means [48]. Furthermore, Beckmann channel model can be described by the following parameters

$$q^2 = \frac{\sigma_{h^I}^2}{\sigma_{h^Q}^2}, \quad r^2 = \frac{\mu_{h^I}^2}{\mu_{h^Q}^2}, \quad k = \frac{\mu_{h^I}^2 + \mu_{h^Q}^2}{\sigma_{h^I}^2 + \sigma_{h^Q}^2},$$
$$\Omega = \mu_{h^I}^2 + \mu_{h^Q}^2 + \sigma_{h^I}^2 + \sigma_{h^Q}^2. \tag{48}$$

As in Rician fading model, the parameter K indicates the ratio between the LoS and non-LoS power. Moreover, as in Hoyt (Nakagami-q) fading model q^2 measures the power imbalance between the quadrature non-LoS components. The parameter r^2 indicates the power imbalance between quadrature LoS components. Finally, the parameter Ω indicates the average power of the fading channel. Table. 1 shows the relation between Beckmann fading model and other fading models in the literature.

REFERENCES

[1] E. Dahlman, G. Mildh, S. Parkvall, J. Peisa, J. Sachs, and Y. Selén, "5G radio access," *Ericsson Rev.*, vol. 6, pp. 2–7, 2014.

[2] E. Basar, M. Wen, R. Mesleh, M. D. Renzo, Y. Xiao, and H. Haas, "Index modulation techniques for next-generation wireless networks," *IEEE Access*, vol. 5, pp. 16 693–16746, 2017.

[3] Q. Li *et al.*, "MIMO techniques in wimax and lte: A feature overview," *IEEE Commun. Mag.*, vol. 48, no. 5, pp. 86–92, May 2010.

[4] R. Mesleh, H. Haas, C. W. Ahn, and S. Yun, "Spatial modulation - a new low complexity spectral efficiency enhancing technique," in *Proc. 1st Int. Conf. Commun. NetW.*, China, Oct. 2006, pp. 1–5.

[5] A. Garcia-Rodriguez and C. Masouros, "Low-complexity compressive sensing detection for spatial modulation in large-scale multiple access channels," *IEEE Trans Commun.*, vol. 63, no. 7, pp. 2565–2579, Jul. 2015.

[6] P. Yang, M. D. Renzo, Y. Xiao, S. Li, and L. Hanzo, "Design guidelines for spatial modulation," *IEEE Commun. Surv. Tut.*, vol. 17, no. 1, pp. 6–26, Jan.–Mar. 2015.

[7] M. Wen *et al.*, "A survey on spatial modulation in emerging wireless systems: Research progresses and applications," *IEEE J. Sel. Areas Commun.*, vol. 37, no. 9, pp. 1949–1972, Sep. 2019.

[8] R. Mesleh, S. S. Ikki, and H. M. Aggoune, "Quadrature spatial modulation," *IEEE Trans. Veh. Technol.*, vol. 64, no. 6, pp. 2738–2742, Jun. 2015.

[9] J. Li, S. Dang, Y. Yan, Y. Peng, S. Al-Rubaye, and A. Tsourdos, "Generalized quadrature spatial modulation and its application to vehicular networks with NOMA," *IEEE Trans. Intell. Trans. Syst.*, pp. 1–10, 2020.

[10] J. Li, M. Wen, X. Cheng, Y. Yan, S. Song, and M. H. Lee, "Generalized precoding-aided quadrature spatial modulation," *IEEE Trans. Veh. Technol.*, vol. 66, no. 2, pp. 1881–1886, Feb. 2017.

[11] Z. Yigit and E. Basar, "Low-complexity detection of quadrature spatial modulation," *Electron. Lett.*, vol. 52, no. 20, pp. 1729–1731, 2016.

[12] L. Xiao, P. Yang, S. Fan, S. Li, L. Song, and Y. Xiao, "Low-complexity signal detection for large-scale quadrature spatial modulation systems," *IEEE Commun. Lett.*, vol. 20, no. 11, pp. 2173–2176, Nov. 2016.

[13] D. K. Nguyen and H. Ochi, "On the impact of transceiver impairments to cognitive df relay networks," in *Proc. IEEE Asia Pacific Conf. Circuits Syst.*, Nov. 2014, pp. 125–128.

[14] O. Semiari, B. Maham, and C. Yuen, "On the effect of I/Q imbalance on energy detection and a novel four-level hypothesis spectrum sensing," *IEEE Trans. Veh. Technol.*, vol. 63, no. 8, pp. 4136–4141, Oct. 2014.

[15] L. Anttila, M. Valkama, and M. Renfors, "Circularity-based I/Q imbalance compensation in wideband direct-conversion receivers," *IEEE Trans. Veh. Technol.*, vol. 57, no. 4, pp. 2099–2113, Jul. 2008.

[16] M. Valkama, M. Renfors, and V. Koivunen, "Advanced methods for I/Q imbalance compensation in communication receivers," *IEEE Trans. Signal. Process.*, vol. 49, no. 10, pp. 2335–2344, Oct. 2001.

[17] J. Zhu, D. W. K. Ng, N. Wang, R. Schober, and V. K. Bhargava, "Analysis and design of secure massive MIMO systems in the presence of hardware impairments," *IEEE Trans. Wireless Commun.*, vol. 16, no. 3, pp. 2001–2016, Mar. 2017.

[18] B. Selim *et al.*, "Performance analysis of single carrier coherent and noncoherent modulation under I/Q imbalance," in *Proc. IEEE 87th Veh. Tech. Conf. (VTC Spring)*, Jun. 2018, pp. 1–5.

[19] E. Hossain and M. Hasan, "5 G cellular: Key enabling technologies and research challenges," *IEEE Instrum. Meas. Mag.*, vol. 18, no. 3, pp. 11–21, Jun. 2015.

[20] D. K. Nguyen and H. Ochi, "Transceiver impairments in DF/AF dual-hop cognitive relay networks: Outage performance and throughput analysis," in *Proc. IEEE 81st Veh. Technol. Conf. (VTC Spring)*, May 2015, pp. 1–5.

[21] D. K. Nguyen, D. N. K. Jayakody, and H. Ochi, "Soft information relaying with transceiver hardware impairments in cognitive networks," in *Proc. 10th Int. Conf. Inf. Commun. Signal. Process.*, Dec. 2015, pp. 1–5.

[22] S. Solanki, P. K. Upadhyay, D. B. da Costa, P. S. Bithas, A. G. Kanatas, and U. S. Dias, "Joint impact of RF hardware impairments and channel estimation errors in spectrum sharing multiple-relay networks," *IEEE Trans. Commun.*, vol. 66, no. 9, pp. 3809–3824, Sep. 2018.

[23] S. Javed, O. Amin, S. S. Ikki, and M. Alouini, "On the achievable rate of hardware-impaired transceiver systems," in *Proc. GLOBECOM IEEE Glob. Commun. Conf.*, Dec. 2017, pp. 1–6.

[24] G. M. Matalkah, J. M. Sabatier, and M. M. Matalgah, "A generalized likelihood ratio test for detecting targets in multiple-band spectral images with improper complex Gaussian noise," in *Proc. 15th IEEE Int. Conf. Image Process.*, Oct. 2008, pp. 1856–1859.

[25] A. S. Aghaei, K. N. Plataniotis, and S. Pasupathy, "Maximum likelihood binary detection in improper complex Gaussian noise," in *Proc. IEEE Int. Conf. Acoust., Speech Signal Process.*, Mar. 2008, pp. 3209–3212.

[26] S. Sallem, J. Delmas, and P. Chevalier, "Optimal SIMO MLSE receivers for the detection of linear modulation corrupted by noncircular interference," in *Proc. IEEE Stat. Signal Process. Workshop*, Aug. 2012, pp. 840–843.

[27] R. Mesleh, S. S. Ikki, and O. S. Badarneh, "Impact of cochannel interference on the performance of quadrature spatial modulation MIMO systems," *IEEE Commun. Lett.*, vol. 20, no. 10, pp. 1927–1930, Oct. 2016.

[28] R. Mesleh and S. S. Ikki, "On the impact of imperfect channel knowledge on the performance of quadrature spatial modulation," in *Proc. IEEE Wireless Commun. Netw. Conf.*, Mar. 2015, pp. 534–538.

[29] R. Mesleh and A. Younis, "LOS millimeter-wave communication with quadrature spatial modulation," in *Proc. IEEE Int. Symp. Signal Process. Inf. Technol.*, Dec. 2016, pp. 109–113.

[30] A. Younis, N. Abuzgaia, R. Mesleh, and H. Haas, "Quadrature spatial modulation for 5 G outdoor millimeter-wave communications: Capacity analysis," *IEEE Trans. Wireless Commun.*, vol. 16, no. 5, pp. 2882–2890, May 2017.

[31] N. Kolomvakis, M. Matthaiou, and M. Coldrey, "IQ imbalance in multiuser systems: Channel estimation and compensation," *IEEE Trans. Commun.*, vol. 64, no. 7, pp. 3039–3051, Jul. 2016.

[32] A. E. Canbilen, M. M. Alsmadi, E. Basar, S. S. Ikki, S. S. Gultekin, and I. Develi, "Spatial modulation in the presence of I/Q imbalance: Optimal detector amp; performance analysis," *IEEE Commun. Lett.*, vol. 22, no. 8, pp. 1572–1575, Aug. 2018.

[33] A. E. Canbilen, S. S. Ikki, E. Basar, S. S. Gultekin, and I. Develi, "Joint impact of I/Q imbalance and imperfect CSI on SM-MIMO systems over generalized Beckmann fading channels: Optimal detection and Cramer-Rao bound," *IEEE Trans. Wireless Commun.*, vol. 19, no. 5, pp. 3034–3046, May 2020.

[34] R. Mesleh, S. S. Ikki, and F. S. Almehmadi, "Impact of IQ imbalance on the performance of QSM multiple-input-multiple-output system," *IET Commun.*, vol. 10, no. 17, pp. 2391–2395, 2016.

[35] E. Basar, U. Aygolu, E. Panayirci, and H. V. Poor, "Performance of spatial modulation in the presence of channel estimation errors," *IEEE Commun. Lett.*, vol. 16, no. 2, pp. 176–179, Feb. 2012.

[36] CISCO, "IEEE 802.11ax: The sixth generation of Wi-Fi," 2020. [Online]. Available: https://www.cisco.com/c/dam/en/us/products/collateral/wireless/white-paper-c11-740788.pdf

[37] R. Want, B. N. Schilit, and S. Jenson, "Enabling the Internet of Things," *Computer*, vol. 48, no. 1, pp. 28–35, Jan. 2015.

[38] M. Gavell, "Advanced analog MMICs for mm-Wave communication and remote sensing in 0.15 μm mHEMT technology," *Chalmers Univ. Technol.*, 2013.

[39] I. Barhumi and M. Moonen, "Frequency-domain IQ-imbalance and carrier frequency offset compensation for OFDM over doubly selective channels," in *Proc. 14th Eur. Signal Process. Conf.*, Sep. 2006, pp. 1–5.

[40] E. Ollila, "On the circularity of a complex random variable," *IEEE Signal. Process. Lett.*, vol. 15, pp. 841–844, 2008.

[41] J. G. Proakis, "Digital communications through fading multipath channels," *Digit. Commun.*, pp. 824–825, 2001.

[42] A. A. Mohsenipour, "On the distribution of quadratic expressions in various types of random vectors," *Electron. Thesis Diss. Repository, Univ. Western Ontario*, vol. 955, pp. 1–164, 2012.

[43] B. Baldessari, "The distribution of a quadratic form of normal random variables," *Ann. Math. Statist.*, vol. 38, no. 6, pp. 1700–1704, 1967.

[44] E. Ollila, J. Eriksson, and V. Koivunen, "Complex elliptically symmetric random variables generation, characterization, and circularity tests," *IEEE Trans. Signnal. Process.*, vol. 59, no. 1, pp. 58–69, Jan. 2011.

[45] S. Kotz, N. Balakrishnan, and N. L. Johnson , "Continuous multivariate distributions," in *Volume 1: Models and Applications*, John Wiley & Sons, 2004.

[46] P. Beckmann, "Statistical distribution of the amplitude and phase of a multiply scattered field," *J. Res. Nat. Bur. Standards, 66D*, vol. 3, pp. 231–240, 1962.

[47] P. Beckmann, "Rayleigh distribution and its generalizations," *Radio Sci. J. Res. NBS/USNC-URSI*, vol. 68, no. 9, pp. 927–932, 1964.

[48] M. Rangaswamy, D. D. Weiner, and A. Ozturk, "Non-gaussian random vector identification using spherically invariant random processes," *IEEE Tran. Aerosp. Electron. Syst.*, vol. 29, no. 1, pp. 111–124, Jan. 1993.

MALEK M. ALSMADI received the B.S. degree from the Department of Electrical and Computer Engineering, The Hashemite University, Zarqa, Jordan, in 2003, the M.S. degree from the Department of Electrical and Computer Engineering, University of Kebangsaan Malaysia, Kuala Lumpur, Malaysia, in 2013, and the Ph.D. degree from the Department of Electrical Engineering, Lakehead University, Thunder Bay, ON, Canada. He is currently a Postdoctoral Researcher with Lakehead University. He was a Professional Computer Trainer with Technical and Vocational Training Corporation, Sakakah, Saudi Arabia, from 2004 to 2012, and a Senior Lecturer with Imam Abdulrahman Bin Faisal University, Dammam, Saudi Arabia, from 2014 to 2016. He also was a Graduate Assistance and contract Lectures with Lakehead University. His research interests include MIMO systems, spatial modulation, NOMA systems, and visible light communication. He is a Reviewer of the IEEE TRANSACTIONS ON INFORMATION THEORY, IEEE SYSTEMS JOURNAL, IEEE ACCESS, and IEEE COMMUNICATIONS LETTERS.

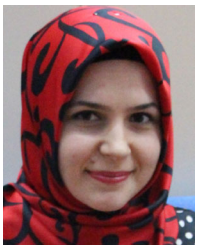

AYSE ELIF CANBILEN received the B.S. and M.S. degrees in electrical and electronics engineering from Selçuk University, Konya, Turkey, in 2012 and 2015, respectively, and the Ph.D. degree in electrical and electronics engineering from Konya Technical University, Konya, Turkey, in 2019. From 2017 to 2018, she was with the Department of Electrical Engineering, Lakehead University, Thunder Bay, ON, Canada, as a Visitor Researcher. She is currently an Assistant Professor with the Department of Electrical and Electronics Engineering, Konya Technical University. Her primary research interests include MIMO systems, spatial modulation techniques, cooperative communications, cognitive radio systems, and reconfigurable intelligent surfaces. She is a Reviewer of the IEEE TRANSACTIONS ON COMMUNICATIONS, the IEEE TRANSACTIONS ON WIRELESS COMMUNICATIONS, the IEEE TRANSACTIONS ON VEHICULAR TECHNOLOGY, the IEEE COMMUNICATIONS LETTERS, and IEEE ACCESS.

NAJAH ABU ALI received the B.Sc. and M.Sc. degrees in electrical engineering from The University of Jordan, Amman, Jordan and the Ph.D. degree from the Department of Electrical and Computer Engineering, Queen's University, Kingston, ON, Canada, specializing in resource management in computer networks. She is currently a Professor with the College of Information Technology, United Arab Emirates University, Al Ain, UAE. Her work has been consistently authored or coauthored in key publications venues for journals and conferences. She has coauthored a Wiley book on 4G and beyond cellular communication networks. Her general research interests include modeling wireless communications, resource management in wired and wireless networks, and reducing the energy requirements in wireless sensor networks. More recently, she has strengthened her focus on the Internet of Things, particularly at the nano-scale communications, in addition, vehicle-to-vehicle networking. She has also delivered various seminars and tutorials at flagship IEEE Communication Societies. She is an Associate Editor of several journals. She was a Reviewer for many noted journals, a TPC member and reviewer in several conferences, and contributed to the organization of several SIs and workshops. She was also the Publication Co-Chair of IEEE GC'18, GC'22.

SALAMA S. IKKI received the Ph.D. degree in electrical engineering from Memorial University, St. Johns, NL, Canada, in 2009. From February 2009 to February 2010, he was a Postdoctoral Researcher with the University of Waterloo, Waterloo, ON, Canada. From February 2010 to December 2012, he was a Research Assistant with the INRS at the University of Quebec, Montreal, QC, Canada. He is currently an Associate Professor of wireless communications with Lakehead University, Thunder Bay, ON, Canada. He is the author of more than 100 journal and conference papers and has more than 4500 citations and an H-index of 32. His research interests include cooperative networks, multiple-input-multiple-output, spatial modulation, and wireless sensor networks. He was on the Editorial Board for IEEE COMMUNICATIONS LETTERS and Institution of Engineering and Technology Communications. He was a Technical Program Committee Member for various conferences, including the IEEE International Conference on Communications, the IEEE Global Communications Conference, the IEEE Wireless Communications and Networking Conference, the IEEE Spring/Fall Vehicular Technology Conference, and the IEEE International Symposium on Personal, Indoor, and Mobile Communications. He was the recipient of the Best Paper Award for what he published in the *EURASIP Journal on Advanced Signal Processing*. He was also recipient of the IEEE COMMUNICATIONS LETTERS, IEEE WIRELESS COMMUNICATIONS LETTERS, IEEE TRANSACTIONS ON VEHICULAR TECHNOLOGY, and IEEE TRANSACTIONS ON COMMUNICATIONS Exemplary Reviewer Certificates for 2012, 2012 and 2014, respectively.